New insights into the Holocene development history of a Pacific, low-lying coral reef island: Takapoto Atoll, French Polynesia

Lucien F. Montaggioni, Bernard Salvat, Annie Aubanel, Edwige Pons-Branchu, Bertrand Martin-Garin, Arnaud Dapoigny, Lydie Goeldner-Gianella

New insights into the Holocene development history of a Pacific, low-lying coral reef island: Takapoto Atoll, French Polynesia

Lucien. F. Montaggioni [a *], Bernard Salvat [b], Annie Aubanel [c], Edwige Pons-Branchu [d], Bertrand Martin-Garin [a], Arnaud Dapoigny [d], Lydie Gianella [e]

Addresses

[a] Aix Marseille Univ, CNRS, IRD, Coll France, CEREGE, 13331 Marseille, France

[b] PSL-École pratique des hautes études (EPHE), USR3278, Labex Corail, Université de Perpignan, 66000 Perpignan, France

[c] Environmental Consultant, BP 2038 Papeete, 98713 Tahiti, Polynésie Française

[d] LSCE/IPSL, CEA–CNRS–UVSQ, Université Paris-Saclay, 91198 Gif-sur-Yvette, France

[e] Paris 1 Univ, UMR CNRS 8591, Laboratory of Physical Geography, F-92195 Meudon cedex, Fance

[*] Corresponding author

Email address: montaggioni@cerege.fr

Highlights

– Initiation of low-lying islets from Takapoto Atoll (French Polynesia) started not prior 2,300 yr BP from isolated depocentres.

– Development of atoll islets occurred mainly throughout a sea-level fall between 2,600 yr BP and the last 500 years.

– Over the last 2,000 years, in northwest Tuamotu islands, cyclone activity was probably more intense from the 11th to 19th century.

Abstract

Low-lying atoll islands are known to be made up of unconsolidated, coral-rich, detritus, together with high amounts of foraminifera, derived from both outer-reef and lagoonal environments. While regarded as highly vulnerable to ongoing global changes, these islands are poorly constrained in term of developement history. Herein is presented a detailed chronostratigraphic study of Tuamotu atoll islands (French Polynesia, south central Pacific) based on analyses of sedimentary sequences through seven excavations along two transects across both windward and leeward rim areas around Takapoto Atoll. The island accretionary chronology is supported by radiometric dating of 62 coral and molluscan clasts. The sequences range between 3.80 m and 1.20 m in thickness, from the oceanic shoreline lagoonwards. Four lithofacies were identified from sediment composition and texture: a coral (pocilloporid)-rich, gravel-supported, preferentially located in the outermost rim areas; a coral-rich, gravelly sand-supported, locally interbedded with gravel-supported units; a foraminifera (amphisteginid)-rich, sand-dominated, mainly located at the central and innermost rim settings; and an organic-rich, sand facies atop of some sequences. A model of atoll islet formation is drawn up in relation to mid to late Holocene sea-level changes. The foundations of islets (motus), namely *conglomerate platforms*, started to form with deposition of patchy, rubble spreads over the upper reef-rim surfaces from ca 4,500 yr BP as sea level was about 0.80 m above its present mean level. On these platforms, islets started to accrete not before ca 2,300 yr BP, from isolated depocentres located midway between outer-reef and lagoon margins. At that time, sea level at about +0.60 m above present mean sea level was starting to slowly decrease to its present position. The major growth phases occurred in a context of continued sea-level fall. Islets continued to accrete through concentric ridges mainly until the last 300 years. Accretion was dominantly driven by low-frequency, high-energy wave-surge events. From dating of coral clasts, a number of one to two events by century were identified as having apparently contributed to island formation at Takapoto. Regionally predicted increase in the rates of sea-level rise may have negative impacts on such islands since these have evolved under conditions of falling sea level.

Keywords: Holocene, southern tropical Pacific, Tuamotu islands, U-Th dating, atoll-island accretion.

1. Introduction

Atolls are mid-ocean, subcircular to elongate coral reefs. The emergent part of the atoll, so-called *atoll reef rim,* is usually covered by dominantly detrital, unconsolidated islets with low elevations, usually less than 5 m in French Polynesia (Duvat et al., 2017) and small spatial extent (a few dozen to hundred square kilometres).

As emphasized by the IPCC (Nurse et al., 2014), such low-lying reef islands are probably among the most sensitive and vulnerable lands to the impacts of climate change, especially to future sea-level rise and increasing storm intensity. The dynamics and hability of atoll islands in the face of the future climatic constrains is therefore of major concern as many atolls are inhabited (Dickinson, 2009; Storlazzi et al., 2015, 2018, East et al., 2018; Kench et al., 2018; Beetham and Kench, 2018).

Understanding the vulnerabilty and expecting the trajectories of habitable atoll territories can come inevitably through detailed historical reconstructions of controls, modes and timings of atoll island development (East et al., 2018; Montaggioni et al., 2018). While special attention has been paid to drivers and modalities of atoll shoreline adjustments in response to the rise in sea level over the last century (Aslam and Kench, 2017; Duvat et al., 2017; Kench et al, 2015, 2018), atoll-island morphodynamic responses to environmental changes at the millennial scale are poorly documented. Available radiochronologically constrained reconstructions of atoll island formation indicate that there are significant interregional differences (Perry et al., 2011) and probably intraregional ones (East et al., 2018), particularly in French Polynesia (Hallmann et al., 2018; Montaggioni et al., 2018).

However, detailed studies on how and when atoll islands have formed in the region are essentially non-existent. A preliminary study on the mode and timing of atoll island development in French Polynesia was recently published (Montaggioni et al., 2018). It was based on the chronostratigraphic analysis of one single windward, south-eastern site at Takapoto Atoll, in the north-western part of the Tuamotu Archipelago. From an ocean-facing, 4 m-deep excavation through a coral-rubble ridge and uranium-series dating of 21 coral clasts, the successive island accretionary stages were identified. The outer part of the island appeared to be composed of three gravelly sand-supported to gravel dominated units that have started to accrete by approximately 1,000 yr BP as sea level was about +0.40 m above present mean sea level (pmsl). The ocean-facing ridge rests on an indurated conglomerate platform, the top surface of which is at present culminating at about +0.50 m. The platform is presumed to have deposited and cemented from 2,000 to around 1,000 yr BP during the time of sea

level drop from +0.60 m to +0.40 m, according to the sea-level curve by Hallmann et al. (2018). Additional dating of surficial coral clasts revealed that, along the south-eastern side of Takapoto, islets tend to initiate and accrete from the inner rim parts oceanwards.

However, this study did not permit to wholly understand the processes of atoll island deposition. At first glance, there is no reason to support the idea that modes and timings of islet development are similar between windward and leeward atoll sides, since there are marked differences between both settings in water-energy regimes, related sediment supplies and rim to forereef-slope morphologies as well (Montaggioni et al., 2019).

The aim of the present paper is to provide detailed stratigraphic analyses of islands from Takapoto Atoll, on windward, south-eastern and leeward, south-western parts. Island stratigraphy is delineated from the chronostratigraphy analysis of seven excavations through ocean- to lagoon-facing sites, based on uranium-series dating of 61 coral clasts and accelerator mass spectrometry radiocarbon dating of one molluscan shell sample. These new datasets allow the conceptual model of atoll-rim island development previously outlined from Takapoto Atoll (Montaggioni et al., 2018) to be improved. Critical episodes and depositional modes of island accretion are identified and interpreted in relation to Holocene sea level fluctuations.

2. Environmental setting

2.1. Atoll location and morphology

Located in the central south Pacific, the Tuamotu Archipelago is comprised of 77 atolls and extends over 1500 km along W–NW to E–SE oriented volcanic chains. Takapoto Atoll is sited in the north-western portion of the Tuamotu, between 14°33''–14°43'' south latitude and 145°08''–145°16'' west longitude (Fig. 1A). It belongs to a specific group of actively subsiding atolls on the Tuamotu Plateau (Dickinson, 2004; Montaggioni et al., 2019). About 17 km long and 5.5 km wide, elliptical in shape, Takapoto is elongated along a SW–NE direction, and covers a total surface area of 74 km^2 (Fig. 1B). The almost continuous, low-lying, atoll rim, about 23 km^2 in total areal coverage, approximates 350 m in width, and entirely encloses a lagoon deeper than 45 m (Chevalier et al., 1979; Salvat, 1981; Salvat and Richard, 1985). The rim is covered by individual islets, known as *motus* in the Polynesian Pacific, reaching 4 m in maximum elevation above present mean sea level (pmsl). Passes are totally missing. The reef islets are elongate or crescent-shaped, usually composed of unlithified coral rubble, mixed with skeletal sands and, on the north-western and north-eastern atoll zones, separated by inter-

101 islet, shallow channels – so-called *hoas* –, shoaling locally at low tide and allowing water exchange between the
102 open sea and the lagooon at high tide. Islets are usually bordered by shingle ridges along the ocean-facing side of
103 the atoll rim. Transverse profiles across both sides of the atoll show similar topographies with a seaward
104 protruding relief (i.e. a ridge) changing into flat to gently dipping benches lagoonwards. Essentially in the
105 middle parts of the windward rim, there are locally shallow swales and ponds. Islets rest usually on coarse-
106 grained, firmly cemented skeletal sheets, forming the so-called antecedent *conglomerate pavements* or
107 *conglomerate platforms*, standing 0.30 m to up to 0.60 m above pmsl (Montaggioni and Pirazzoli, 1984;
108 Pirazzoli and Montaggioni, 1986, 1988; Montaggioni et al., 2018). Previously published radiometric dating of
109 conglomerates at Takapoto revealed that these have deposited between 6,609 ± 55 and not earlier than 1,019 ± 4
110 yr BP (Montaggioni et al., 2018), prior to be cemented within phreatic and vadose marine zones during a period
111 of higher than present sea level (Montaggioni and Pirazzoli, 1984).

112 The outermost parts of the atoll rim are fringed by a living coral reef tract. This comprises a reef-flat zone, about
113 100 to less than 50 m wide, less than 1 m deep at low tide. The reef flat is followed seawards by a spur-and-
114 groove system sloping down to the depth of around 10 m and capped by an algal ridge, 0.20–0.50 m high at its
115 inner border, especially at the windward, eastern settings (Chevalier et al., 1979; Bouchon, 1983; Salvat and
116 Richard, 1985; Külhman and Chevalier, 1986). This system ends either into a gently or steeply dipping foreslope
117 to depths greater than 35 m depending on the location (Montaggioni et al., 2019). The atoll islets are known to
118 be supplied mainly with coral detritus from communities living on adjacent reef-flats and upper forereef zones to
119 depths of about 20 m (Harmelin-Vivien, 1994; Harmelin-Vivien and Laboute, 1986) and from lagoonal deposits
120 in their innermost portions (Adjas, 1988). The relevant coral communities are dominated by robust-branching
121 *Pocillopora* and massive *Porites* (Bouchon, 1983; Külhmann and Chevalier, 1986; Montaggioni et al., 2019).

122 *2.2. Climate*

123 The climate in the north-western Tuamotu region is of tropical type. The warm, rainy, austral summer lasts from
124 November to April and the relatively cooler and dryer, austral winter from May to October. Air temperature
125 varies between 23 °C and 30 °C. Rainfall approximates 1500 mm/year. The tide regime is microtidal and semi-
126 diurnal, averaging 0.5 m in amplitude to a maximum of 0.70 m at spring tide.

127 The regional climate system is both driven by the trade-winds and by El Niño-Southern Oscillation (ENSO)
128 which regulates tropical to extra-tropical storms (Andréfouët et al., 2012). Takapoto Atoll experiences the effects

of trade-winds, blowing from the E–NE sectors for 70 % of the year and from the SE for 20 %. In the austral winter, the sea conditions are driven by strong trade-winds and southern swells resulting in a high-energy wave regime. Periods of low wave heights (around 1.5 m) and calm occur between periods of moderate to high swells (2.5 m). During the austral summer, the wave regime is typified by low wave heights (Andréfouët et al., 2012). Trade-winds are significantly less active and generate moderate-energy wave conditions, locally disturbed by high-energy events initiated either by ENSO-related cyclones or by storms originating from northern latitudes. Higher amplitude waves (up to 3.75 m) can be generated by three event types: high easterlies winds, western transient storms and distant cyclones (Andrefouët et al., 2012). The cyclonic season usually extends from November to April, with a large annual variability mainly related to ENSO. The eastward migration of warmer sea surface temperatures during El Niño episodes promotes the displacement of tropical storms further east into the the Tuamotu region. The cyclone track pattern in French Polynesia is typified by a tapering channel between the Society and the Austral Islands through which 70 % of the cyclone tracks pass (Larrue and Chiron, 2010).

Events of extreme wave hazard are poorly documented in the Tuamotu region. Lau et al. (2016) provided a comprehensive survey of recorded cyclones and their effects in historical times. A total of about 24 cyclones are known from the Tuamotu for the past 192 years between 1822 and 2014. The north-western Tuamotu islands were occasionally visited by tropical storms and cyclones (4–10 per century; Dupon, 1987) with maximum wind gusts up to 150 km/h and swells higher than 6 m. Since the beginning of the 20th century, Takapoto has been hit by four cyclones (Duvat et al., 2017 and references therein). Over periods of several centuries, the number of cyclonic events in the northwestern Tuamotu have probably not exceeded 2–3 per century (Canavesio, pers.com.). Gaps of longer than 100 years are not uncommon between extreme wave events. However, such events seem to have been of greater magnitude during the past than during the last century (Lau et al., 2016). While the cyclonic hazard in the region is typified by a very low frequency of events, it displays active phases mainly in relation with ENSO episodes, during which several cyclonic events can occur within short time intervals. Cyclone hazard records reveal a 50-year return period for wave exceeding 12 m high (Canavesio, 2014).

Little is known about the effects of cyclones and storms in shaping atoll morphology. In 1906, on Anaa Atoll, cyclone-generated waves have removed the western side of the island over a distance of more than 300 m. Canavesio (2014) estimated that these waves have reached heights ranging between 15.5 m and 18.5 m. From 1926 to 2010, a total of 50 cyclones were registered in French Polynesia, but only those of 1982–1983 and 1997–1998 resulted in severe disturbances fore-reef coral communities at Takapoto (Harmelin-Vivien and

159 Laboute, 1986). During Cyclone Orama, in February 1983, the village was flooded by 4 m to 5 m high waves.
160 Laboute (1985) pointed out that about 50 to 100 % of the living fore-reef coral communities were destroyed
161 along the eastern side of the atoll at that time.

162 As for the cyclone activity, little information is available on the frequency and effects of tsunamis in the
163 Tuamotu (Etienne, 2012). The available data suggest that, since the 16th century, the Tuamotu islands were
164 affected by less than ten tsunamis generating 0.3 m to 1.9 m-high waves (Lau et al., 2016). Based on numerical
165 modeling and direct observations, the Tuamotu region seems to have not been significantly affected by tsunami
166 waves compared to high volcanic French Polynesian islands (Sladen et al., 2007).

167 Recontruction of absolute sea-level changes in the tropical Pacific over a 60-year period (1950–2009) indicated
168 that sea level rose by 2.5 ± 0.5 mm/yr, a value higher than the mean global absolute sea-level rise (1.2 to
169 1.8 mm/yr) estimated for the 20th century (Becker et al., 2012). For the next decades, models predict an
170 acceleration of sea-level rise in the north-western Tuamotu atolls, with rates greater than 8 mm/yr (Botella,
171 2015).

172 **3. Materials and methods.**

173 *3.1. Field work*

174 Topography surveys were conducted along two transects, respectively across the south-eastern and south-
175 western sides of the reef rim (Figs. 1B, 1C and 2). Behind a 100-m wide reef-flat zone, the south-eastern transect
176 extends over 330 m, from the ocean-facing shoreline to the lagoonal border (Figs. 1C and 2), between
177 S14°40'42"–W145°12'50" and S14°40'41"–W145°12'57''. Behind a 60-m wide reef-flat zone, the south-
178 western transect extends over 370 m inland (Figs. 1D and 3), between S14° 41'08"–W145°15'32" and
179 S14°41'14" and W145°15'20". Levelling was undertaken using a conventional automatic level. Along the
180 transect, each reference point was positioned using DGPS coordinates. Rim elevations were established by
181 reference to present mean sea level, assuming a conservative error of ±0.10 m.The island surfaces are densely
182 covered by coconut plantations.

183 Island topography on south-eastern, windward and south-western, leeward sides are comparable. Alongside the
184 ocean, both transects exhibit unconsolidated rubble ridges, running parallel to the shoreline, with ocean-facing

steep (30°–45°) scarps. Ridges culminate at elevations of about 4.10 m and 3.30 m above pmsl at the eastern and western settings respectively. Behind the ridges, there are flat-topped benches, spreading out over 200 m lagoonwards and culminating at mean heigths of about 1.5 m to 1.80 m. The benches end into 20–10° sloping, beaches, less than 20 m wide, lagoon side.

Vertical excavations using backhoe were dug in both transects from top surface to underlying conglomerate surfaces in order to determine island subsurface stratigraphy. Starting from outer ridges inwards, surveys were conducted, at the south-eastern, windward atoll side, from four excavations, successively labelled A, B, C and E (Fig. 2), and at the south-western, leeward side, from three others F, G, and H (Fig. 3). Excavation location was defined using a GPS positioned at the surface. Field grain-size analysis of coarser detrital material was performed using the Udden-Wentworth classification (Terry and Goff, 2014) as measured along the longest axis from photographed square-metre quadrats. Coral pebbles and coarse-grained were collected for radiometric dating at all excavated sites. Taxonomic identification of dated coral and molluscan specimens was made at the generic level.

3.2. Radiometric dating procedures.

In order to deternine island chronostratigraphy and accretion history, a total of 62 samples, labelled SAT – according to B. Salvat, collector – were collected along the walls and at the bottom of the excavations. Only one sample composed of sand-sized molluscan shelly debris (SAT 97A2) was dated using the AMS radiocarbon method at the LMC 14 – Laboratoire de mesure du carbone 14 –, ARTEMIS National Facility at Gif-sur-Yvette, France. A radiocarbon age of 2,725 ± 30 was returned. Calibration using the IntCal13 and Marine13 radiocarbon calibration programme (Reimer et al., 2013) yielded a calibrated age of 2,447 ± 127 with a two sigma error range.

For U/Th analysis purposes, millimetric pieces of coral clasts were cut using a micro saw in order to select the most clean and pristine parts. These pieces were rinsed with mQ water and ultrasonicated several time.

After adding a triple ^{229}Th ^{233}U–^{236}U spike in a Teflon beaker, samples (from 150 to 350 mg) were dissolved with diluted HCl. The U-Th separation and purification were performed after coprecipitation with $Fe(OH)_3$, on 0.6 ml columns filled with U-TEVA and pre-filter resins, in nitric media – see Pons-Branchu et al., 2014 for details. The U and Th isotopic compositions were analyzed at the *Laboratoire des Sciences du Climat* (LSCE,

France), on a Multi-Collector inductively coupled plasma source mass spectrometer (MC–ICPMS) Thermo Scientific™ Neptune^{Plus} fitted with a desolvating introduction system (aridus II) and a jet interface. For mass fractionation correction, we used an exponential mass fractionation law – normalized to natural $^{238}U/^{235}U$ isotopic ratio –and standard–sample bracketing. More details on the analytical procedure (chemistry and MC-ICPMS analysis) can be found in Pons-Branchu et al. (2014). After corrections for peak tailing, hydrate interference and chemical blanks, $^{230}Th/^{234}U$ ages were calculated (Table 1) from measured atomic ratios through iterative age estimation using the ^{230}Th, ^{234}U and ^{238}U decay constants of Cheng et al. (2013) and Jaffey et al. (1971).

3.3. Establishing island chronology.

The use of U/Th measurements from displaced skeletal material (corals, molluscs, foraminifera) for reconstructing depositional histories of atoll islands were discussed by Woodroffe et al. (1999, 2007), Kench et al. (2014) and Montaggioni et al. (2018). An indefinite time interval (tens to hundreds of years) is postulated to separate the time of death of a given organism from the time of final deposition and stabilisation of its skeletal fragments. Coral clasts may have experienced successive cycles of displacement, reworking and resedimentation. This is clearly evidenced by some age inversions in the stratigraphic sections. Island chronologies have therefore to be regarded as relative, not absolute. However, consistensy of island chronologies is ensured by the fact that most dated samples occupy a stratigraphic position within the excavations which is usually consistent with their age (Figs. 4 and 5). Samples tend to be younger closer to the surface. In a given stratigraphic section, the youngest ages obtained are regarded as closer to the time of definitive stabilisation of the relevant island section.

4. Results

4.1. Lithostratigraphy

All excavations terminated 0.30–0.50 m above pmsl on a firmly cemented, composite surface, composed of gravel-sized, coral clasts embedded within a sandy matrix and identified as the underlying conglomerate platform. Locally, this surface is inundated by the water table at levels higher than of about 0.10 m (excavations C, E and G) to 0.40 m (excavation H). The thicknesses of the overlying, unconsolidated deposits are relatively

comparable within windward and leeward sites, according to their position along the transects. The ocean-facing, windward rubble-ridge sequence (excavation A) is 3.80 m thick (Figs. 2 and 6), while the thickness of the leeward-ridge one (excavation F) does not exceed 3 m (Figs. 3 and 7). The sedimentary sequences from the innermost sites range between 1.20 m and 1.50 m thick (Fig. 8). Except in the windward, outer-ridge sequence that contain sediment layers of about 2 m thick, other sequences are composed of layers averaging 0.20 m to 0.30 m in thickness (Fig. 9). Grain-size decreases from the outermost deposits lagoonwards. Gravel-dominated facies laterally grades into gravelly, sand-supported, then in sand-dominated facies.

Sediment composition and texture are highly consistent between windward and leeward sides. Gravels, including cobbles and pebbles, are dominantly composed of coral pocilloporids, associated with acroporids and faviids, and low amounts of molluscan shells and coralline algal debris. Sandy fractions contain locally up to 80 % of benthic foraminifera. The remaining sand grains come mostly from coral, molluscs and algae. Foraminiferal detritus are almost exclusively composed of *Amphistegina lobifera*, associated with *Marginopora vertebralis*. Subordinate forms include *Sorites, Cymbaloporetta, Amphistegina lessonii* and miliolids.

Four major lithofacies were delineated, primarily based on textural characteristics.

1– Gravel-dominated facies.

It is divided into two subfacies as distinguished by its clast-supported attributes: gravel-supported and sand-supported. Both facies were reported from both atoll sides. Throughout the studied sites, amounts of gravel-sized sediments were markedely higher on the windward than the leeward rim sites. The gravel-supported subfacies is common within all windward holes at different stratigraphic levels (Fig. 9A), to 270 m back from the oceanic shoreline. By contrast, it seems to occur on the leeward coast only in excavation F (Figs. 9B, 9C) where it is most prevalent and at top of excavation G (Fig. 9D), up to 150 m behind the oceanic shoreline. However, this does not imply non-deposition of gravels further inland. The second sand-supported, gravelly subfacies is largely dominant over the gravel-supported one, especially within the south-eastern, windward areas, representing about 90 % of the total sediment volume in excavations A, B and C (Fig. 9D).

Longest axis of coral gravels ranges between 300 mm (fine boulder) and less than 5 mm (fine pebble) with mean values of 100 to less than 10 mm. Along the windward atoll side, the gravel sizes tend to decreases lagoonwards. The mean size varies between 50 and 10 mm in the two outermost sites (excavations A, B) to reach 15 and less than 10 mm in the two innermost (excavations C, E). A similar size-decreasing trend was observed along the

leeward island parts. Gravelly grains are 120 mm in mean size at the ocean-facing site (excavation F), but are sized at an average of 40 and 3 mm in the innermost holes (excavations G, H) respectively. Surprisingly, the biggest gravels, 300 mm in maximum length, were found in the leeward, ocean-facing shingle ridge (excavation F).

The thickness of gravel-dominated stratigraphic units is consistent from site to site, averaging 0.30 to 0.40 m. Grading occurs usually in each unit, with a fining-upward trend. The units are usually separated by erosional, locally lithified surfaces as observed within the outermost, leeward site (excavation F).

2– Sand-dominated facies.

Sandy sediments were deposited mostly in the innermost island areas at both windward and leeward settings, within excavations C, E, G and H (Figs. 10A, 10B, 10C). Sands are usually coarse-to medium-graded (1–0.25 mm in mean size) and well to moderately sorted as mostly composed of larger foraminiferal tests, together with coral and molluscan detritus. Proportions of sand-supported, gravel-sized grains vary locally. As a whole, their proportions tend to increase upwards in the stratigraphic cross-sections. In sand-dominated sequences (excavations E and H), foraminifera-rich layers, about 10–20 mm thick, are distributed in the form of fining-upward, graded-bedding units and alternate with coralgal-rich beds of similar thickness (Fig. 10D).

3– Organic-rich, sand facies.

This facies relates to the development of an organic-rich, brown to black-coloured, root-bearing horizon at the uppermost parts of most sedimentary sequences, mainly at the expense of sand-dominated deposits (Figs. 8B, 8D, 10A, 10B, 11). It is missing from excavations B and F, the top of which consists exclusively of gravel-supported material. Its thickness is relatively constant from one sequence to another at both atoll sides, ranging between 0.3 m and 0.50 m, except atop of hole A where it does not exceed 0.10 m. Sands were primarily coarse-sized, poorly sorted and supporting coral clasts as long as 10 to 50 mm.

4.2. Chronostratigraphy

Corrected ages, expressed as years before 2018 or 2019 (yr BP), range between 70 ± 10 yr BP for Sample SAT 77A (excavation F) and 6.629 ± 38 yr BP for Sample SAT 74 (excavation A) (Table 1). The initial uranium isotopic composition ($\delta^{234}U_i$) range within the modern marine composition (146.86 ± 0.1 ‰ Andersen et al.,

292 2010) within the ±5 ‰ interval usually used as criterion for age reliability, except 3 samples from excavation B
293 (SAT 53A, 60A and 119A) that display values slightly lower (between 136.0 ± 1.9 and 139.2 ± 1.9).

294 Samples from the basal conglomerate platform returned ages ranging from 6,629 ± 38 yr BP (SAT 74A) to
295 2,257 ± 8 yr BP (SAT 101A). The youngest ages at base of the overlying unconsolidated sediments within
296 windward and leeward sites vary between and 2,358 ± 8 yr BP (SAT 93B) and 676 ± 13 yr BP (SAT 73B). At a
297 given site, these are wholly younger than those of conglomerate pavements. In the uppermost stratigraphic
298 sections, ages vary from 2,531 ± 53 yr BP (SAT 96A) to 70 ± 10 yr BP (SAT 77A).

299 Within most of the stratigraphic columns, ages tend to decrease from base to top and accordingly appear to be
300 stratigraphically consistent (Figs. 4 and 5). In the windward and leeward outer-ridge sequences (excavations A
301 and F), ages decrease from 636 ± 7 yr BP (SAT 73A) to 156 ± 12 yr BP (SAT 68A) and from 1,130 ± 10 yr BP
302 (SAT 86B) to 70 ± 10 yr BP (SAT 77A) respectively. Similarly, within holes through the plateaus behind the
303 outer ridges, ages range from 1,660 ± 60 yr BP (SAT 57B) to 1,280 ± 13 yr BP (SAT 52A) in hole B, from
304 2,340 ± 11 yr BP (SAT 36B) in hole C, and from 2,843 ± 16 yr BP (SAT 100A) to 801 ± 13 yr BP (SAT 97A1)
305 in hole H. Hole G is distinguished by the fact tthat the five dated samples returned ages clustered between
306 2,958 ± 17yr BP (SAT 91B) and 2,358 ± 8 ur BP (SAT 93B). Such a narrow age range may express either a
307 rapid accretion of this island part, within a 400 year-long interval or a contiuous supply from a same sediment
308 source. The average time lag between base and top of each sequence can be estimated as follows: 500 years in
309 hole A, 400 years in hole B, 960 years in hole C, 500 years in hole E, 1,000 years in hole F, 600 years in hole G
310 and 1,100 years in hole H.

311 The oldest deposits in both atoll sides were encountered in excavations from the mid rim-parts. Ages range, in
312 hole C, from 2,635 ± 12 yr BP (SAT 34B) to 2,411 ± 15 yr BP (SAT 34A) and, in hole G, from 2,958 ± 17 yr BP
313 (SAT 91B) to 2,358 ± 8 yr BP (SAT 93B). By contrast, the youngest dates from the two transects were reported
314 from the outer-ridge sections, varying between 636 ± 7 yr BP (SAT 73A) and 156 ± 12 yr BP (SAT 68A) at the
315 windward side (excavation A) and 1,130 ± 10 yr BP (SAT 86B) and 70 ± 10 yr BP (SAT 77A) at the leeward
316 side (excavation F). As a summary, across both rim transects, ages tend to progressively decrease from the
317 central excavated sites (C and G) toward the lagoon margin and the ocean respectively.

5. Discussion

5.1. Age of deposition of conglomerate pavements

Ages of coral clasts trapped into conglomerate pavements vary widely from 6,629 ± 38 yr BP (SAT 74A) to 2,600 ± 20 yr BP (SAT 60A) at the windward setting and from 4,683 ± 21 yr BP (SAT 94A) to 2,257 ± 8 yr BP (SAT 101A) at the leeward one, expressing difference in age of about 4,000 and 2,500 years respectively (Table 1; Figs. 2, 3, 6 and 7). Such age discrepencies in basal conglomerate platforms appear to be a common feature in coral islands as reported, for instance, from the Marshall Islands (Kench et al., 2014). At Takapoto, basal conglomeratic material previously extracted from other windard sites provided similar age offsets (Montaggioni and Pirazzoli, 1984). Thus, previous U/Th dating of conglomerates underlying a shingle ridge sitting about 130 m north of the presently studied windward ridge (excavation A) provided ages of 1,391 yr BP to 1,019 yr BP (Montaggioni et al., 2018). This may indicate that coral material accumulated in a same narrow area have been supplied from a same adjacent stock containing detritus reworked over periods of several centuries prior to be deposited and stabilized. An alternative explanation is that deposition of conglomerate clasts is far from having been synchronous throughout the rim and has been rather patchy, originally resulting in the development of isolated, small cells to discontinuous spreads, finally more or less merged as observed at present. Sediment may have been provided by sources applied at different times during the Holocene sea level course. This is in agreement with previous dating of basal rubbles or conglomerates from low-lying islands throughout the Pacific, confirming their deposition mostly during the mid to late Holocene (Chivas et al., 1986; Hayne and Chappell, 2001; Yu et al., 2012; Kench et al., 2014; Montaggioni et al., 2018). According to good coherency of age distribution versus elevation as observed in the different island stratigraphic sequences from both the present study and the previous one (Montaggioni et al., 2018), youngest ages of coral clasts are postulated to be close to time of deposition and represent maximum ages of deposition.

5.2. Age and mode of island development.

Assuming that ages of coral-clast production trapped into conglomerate pavements is very close to that of conglomerate formation, deposition of conglomerates on which islets have settled, would occur within a short interval, between around 2,600 yr BP and 2,200 yr BP on both rim sites, according to their youngest ages (2,257 ± 8 yr BP, SAT 101A; 2,600 ± 20 yr BP, SAT 60A). Islets started to shape relatively coevally from

windward to leeward places. This is supported by ages of the lowermost, youngest deposits in some stratigraphic sequences: 2,340 ± 10 yr BP (SAT 36B) in hole C, 2,843 ± 16 yr BP (SAT 100A) in hole H, 2,358 ± 10 yr BP (SAT 93B) in hole G. The outermost, ocean-facing parts of islets seem to have begun to growth later, presumably from 1,100 - 1,000 yr BP in accordance with ages recorded at base of holes A (636 ± 7 yr BP; SAT 73A) and F (1,130 ± 10 yr BP; SAT 86B). Age distributional patterns (Figs. 2, 3, 6 and 7) revealed clearly that the oldest sections at windward and leeward settings are those located in the central parts of the rim (holes C and G). This gives evidence that islets began to accrete from distinct, nodal locations, interpretated as depocentres, located approximately midway between the ocean-facing beach and lagoon margins, at around 200 and 150 m from the beach, respectively on the windward, eastern and leeward, western sites. From the initial depocentres, proto-islets have presumably continued to develop laterally and both lagoonwards and oceanwards (Figs. 6, 7 and 12). Spaces between the depocentres have probably functioned as zones of water exchange, i.e. paleo-hoas. The final phase of island accretion is believed to relate to infilling of remaining spaces between the outer margin of the depocentres and the innermost parts of the reef-flat zone. The mode of island development was identical on both rim sides as illustrated by isochron distribution (Figs. 6, 7 and 12). However, there is no direct evidence that the entire atoll-island areas were built from an amalgation of a series of neighboring, isolated islets and, similarly, that there was formerly a crenulated shoreline with alternating motus and hoas, with gradual infilling of hoas, since, at present, the island-rim is prominently bounded by a continuous strecht of a linear shoreline. The proposed accretionary island model is based on observations of the present-day topographic status of a number of nearby atoll islands (for instance, Ahe, Manihi). These are composed mainly of a series of small, isolated islets, still separated by functioning hoas. This status may represent an intermediate, immature stage of atoll-island development. In addition, assuming that islet accretion result predominantly from cyclone-generated deposition, every deposit can be spatially restricted, as controlled by the path of the generating cyclone and sustainability of sediment sources.

Islet depocentres were initiated at around 2,300–2,200 yr BP, as expressed by the youngest ages at base of excavations C (2,340 ± 10 yr BP; SAT 36B) and G (2,358 ± 8; SAT 93B). Accretion of the depocentres would have operated throughout approximately 800 years, between 2,300 and 1,500 yr BP. From stabilization time of the depocentres, the development of the main islet parts was complete within about one millennium. The windward, outer shingle ridge would have formed in about 500 years, close to the growth time (700 years) of the outer shingle ridge rising at 130 m further north (Montaggioni et al., 2018). In addition, age comparison between the uppermost parts of outer-ridge sequences (holes A and F) and of innermost ones (holes E and H) gives

375 support to the idea that ocean-facing reliefs, dated from 193 to 70 yr BP at top, experience permanently active
376 reshaping while lagoonward margins may have remained relatively stable since at least the last 500 years.

377 Lateral accretion rates occurred at varying rates along the outer and inner parts of both sides, starting from the
378 central depocentres. The windward, outer rubble ridge developed oceanwards at rates of about 10–15 cm/yr
379 while not higher than 5 cm/yr at the leeward setting. Along both windward and leeward sides, the inner areas
380 would accrete lagoonwards at rates less than 5 cm/yr. These values clearly take into account episodes of
381 erosional and reworking events since major depositional episodes are known to have occurred through
382 instantaneous, low-frequency wave-surge events (see below).

383 *5.3. Frequency of island-shaping, high-energy wave events.*

384 Assuming that island shaping result from deposition of coral clasts mainly derived from upper forereef and reef-
385 flat populations hit by winter storms and cyclones (Bourrouilh-Le Jan and Talandier, 1985; Harmelin-Vivien and
386 Laboute, 1986) and partly from lagoonal areas (Adjas, 1988), attempt can be made to link dated samples to a
387 given extreme hazard events, especially for the last 2,000 year-period (common era, CE), using the recently
388 completed database of cyclone activity in French Polynesia (Laurent and Varney, 2014; Lau et al., 2016;
389 Canavesio et al., 2018). From the U/Th age database provided herein, were identified a total of 25 events, taking
390 into account possible age overlapping between samples as identified by U/Th error range (Table 2). These events
391 are time distributed as follows: only one event from the 1st, 3th, 5th, 4th, 6th, 7th, 11th, 18th, and 20th centuries,
392 two events from the 8th, 13th, 14th, 15th, and 16th centuries, and three events from the 9th and 19th centuries.
393 These findings agree with the fact that cyclone frequency was relatively high in the north Tuamotu from the 11th
394 century, with an average of two extreme wave events per century (Toomey et al., 2013; Montaggioni et al.,
395 2018; Etienne et al., in preparation). The most striking feature relates to age deposition of ocean- and lagoon-
396 facing island areas respectively in relation to wave-surge events (Fig.13). At windward and leeward sites as well,
397 deposition occurred closer to lagoon margins (Excavations B, C, E and H) dominantly between the 1st to 12th
398 centuries. Sediments were mostly composed of sands. By contrast, deposition along outer rim margins
399 (Excavations A and F) took place later, between the 9th and 20th centuries. Sediments were gravel-dominated.
400 In addition, this last episode was coeval with deposition of a number of megaclasts in the Tuamotu (Lau et al.,
401 2016; Canavesio et al., 2018). This may confirm not only an increase in cyclone frequency, but also may reflect
402 an increse in cyclone intensity since the 11th century, resulting in an increasing transport capacity of wave

403 surges.

404 Sample SAT 99B dated back to 53 ± 9.5 CE may have been generated by the same hazard event that has
405 displaced the mega-boulder dated from 54 CE at Kauehi Atoll in north-west Tuamotu (Canavesio et al., 2018).
406 Intense storminess was reported by Nunn (2007) and Toomey et al. (2013) in the central south Pacific over the
407 11th to 15th centuries as recorded by deposition of megaclasts by about 1270, 1300, 1330, 1420–1430 CE at
408 Makemo Atoll, central Tuamotu (Lau et al., 2016). The ages of Samples SAT 71B (1269 ± 16), SAT 73A
409 (1320 ± 12.5), SAT 74 (1344 ± 12.5 CE) encompass this period of high storm activity. Sample SAT 81A dated
410 at 1566 ± 5.5 CE is coeval of two megaclasts deposited on the north-eastern coast of Takapoto (Etienne et al., in
411 preparation). The three wave-surge events recognized in the 19th century, based on Samples SAT 68A
412 (1864 ± 11.5), SAT 77B (1856 ± 4.5) and SAT 68B (1826 ± 10 CE), may be related to cyclones that occurred in
413 1822, 1825, 1877-1878 CE (Lau et al., 2016). These events were also identified by Canavesio et al. (2018) in the
414 central Tuamotu (Marokau and Hikueru Atolls). Sample SAT 77A with an age of 1948 ± 9.5 CE may have been
415 supplied by the January 1958 event, the only registered in the Tuamotu since 1903 for the first half of the 20th
416 century.

417 Going back into the first millennium before Jesus Christ (BC), a number of 11 distinct hazard events were
418 apparently registered. The frequency ranges around 1 to 3 events per century: one over the 10th (940 BC, SAT
419 91B), the 9th (825 BC, SAT 100A), the 7th (620 BC, SAT 34 B), the 3rd (240 BC, SAT 101A) and the second
420 (120 BC, SAT 99A), two or three over the 8th (790–770 BC, SAT 53A, 55A, 57A; 740 BC, SAT 52B), the 6th
421 (590–580 BC, SAT 50A, 55B, 60A; 510 BC, SAT 53B, 96A), and the 4th (390–380 BC, SAT 34A, 93A; 340–
422 350 BC, SAT 91A) centuries. Although, the number of hazard events counted as from simple analysis of the
423 number of clast occurrences can be biased due to random sampling, frequency of high-energy events recorded
424 from the 10th to 2nd centuries BC is quite consistent with that calculated from the CE interval. Accordingly, as a
425 summary, the present study is assumed to confirm that high-energy events would occur in the north Tuamotu
426 over the last 3,000 years at an average frequency of one to two per century with a recurrence time of 50 to 100
427 years. More especially, the increase in cyclone intensity from the 11th century deserves to be emphasized.

428 *5.4. Conceptual model of atoll-island development*

429 Based on a previous chronostratigraphic analysis of one windward, outer shingle ridge excavation at Takapoto,

Montaggioni et al. (2018) postulated that the relevant motu was not emergent prior to about 1,000 yr BP. This assumption remains in line with the present study. However, new records from the seven additional excavations lead to improve the previous atoll-island development model in relation to the mid to late Holocene sea-level oscillations (Fig. 14).

In western French Polynesia, the sea-level course over the last 7,000 years is relatively well constrained from dating of reef cores and elevated micro-atolls, respectively by Bard et al. (1996) and Hallmann et al. (2018). Previous sea-level reconstructions come from petrographical examination of conglomerate platforms, especially at Takapoto (Montaggioni and Pirazzoli, 1984), together with dating of elevated coral heads (Pirazzoli and Montaggioni, 1986, 1988). Thus, it appears that, at around 7,000 yr BP, sea level was approximatelly 10 m below pmsl (Bard et al., 1996). At that time, the late Pleistocene reef surfaces at Takapoto are assumed to have been close to sea level, resulting in colonization by coral communities (Fig. 14A). Sea level outpassed its present position by about 6,000–5,500 yr BP in the Tuamotu (Hallmann et al., 2018) and, especially at Takapoto (Montaggioni and Pirazzoli, 1984; Pirazzoli and Montaggioni, 1986, 1988). As a result of upward accretion over the mid-Holocene, the top of the reef rim was then at depths of about 5–6 m below pmsl (Fig. 14B). Sea level continued to rise up to elevations of +0.80 m to +1 m from 5,000 to 4,000 yr BP (Pirazzoli and Montaggioni, 1988; Hallmann et al., 2018). Assuming a mean vertical accretion of 4–5 mm/yr (Montaggioni, 2005), reef-rim surfaces are thought to have stabilized close to pmsl after a 1,000–1,500 year-long vertical accretion, at about 5,000–4,500 yr BP. High intensity, wave-surge events probably started to supply rim surfaces with significant quantities of coral clasts. From that time, sea level began to drop progressively (Hallmann et al., 1988). From 3,000 to 1,500 yr BP, sea level dropped from about +0.70 m to +0.50 m respective to pmsl (Pirazzoli and Montaggioni, 1986, 1988; Hallmann et al., 2018). According to their youngest ages within the test areas, conglomerate platforms would ended up forming not earlier than 2,300 yr BP, probably as patchily distributed deposits at the outset (Fig. 14C). Conglomerate cementation was interpreted to have occurred within vadose to phreatic zones, presumably from 2,300 to less than 1,000 yr BP according to location, as sea level was sligtly higher than present (Montaggioni and Pirazzoli, 1984), between +0.60 m to +0.30 m. From 1,500 to 1,000 yr BP, sea level dropped regularly toward its present position (Fig. 14D). Correlatively, coral gravels continued to accumulate over conglomerate beds, forming depocentres. These extended laterally forming discontinuous islets. From 1,000 to 500 yr BP, islets develop dominantly oceanwards to finally form an almost continuous island (Fig. 14E). The present configuration of the atoll island was acquired over the last three centuries (Fig. 14F).

459 The degree of exposure of each respective rim side to wave surges, has apparently controlled distances to which
460 deposits were transported from the outer reef margins and the lagoonal slopes. According to the transport
461 capacity of waves (Presto et al., 2006), most coral clasts appear to have been first trapped at respective distances
462 of about 200 m on the south-eastern, windward side and to 150 m on the south-western, leeward side prior to
463 stabilize. As a result, detrital deposits are postulated to have begun to develop in the form of small islets
464 (depocentres), subcircular to elongated, as soon as 2,300–2,000 yr BP. Located initially closer to the lagoon
465 border than to the oceanic coastline, these are regarded to have continued to spread concentrically both
466 oceanwards and lagoonwards during the lowering sea level over the past 1,500 years (Figs. 13D, 13E). Islet
467 extension to lagoon margins seem to have been achieved between about 1,000 and 500 yr BP, while ocean-
468 facing shingle ridges approached the modern oceanic coastline not earlier than 200–100 yr BP (Fig. 13F).
469 Unconsolidated sections of islets have started to develop when sea level was some 0.60–0.50 m above pmsl
470 while conglomeratic foundations were still partly submerged. Consequently, at Takapoto and possibly, in other
471 subsiding north Tuamotu atolls, islands are regarded as having mostly developed during a time of falling sea
472 level.

473 The source of the material extending islets to lagoonward remains questionable, due to the lack of identifiable
474 biogenic tracers exclusively confined to lagoonal environments. For instance, compositional analysis by Adjas
475 (1988) revealed that, at Takapoto, sediments of reef flats and nearby beaches contain about 15% to up to 50% of
476 foraminifera respectively, and those from lagoonal talus and bottoms, about 20%. In all of the studied atoll sites,
477 the foraminiferal assemblages are similarly dominated by *Amphistegina* and *Marginopora*, thus making difficult
478 the sediment sources to be identified. It is hypothesized that cyclones are able to remove and redeposit most
479 sand-graded bioclasts derived from both ocean-facing and lagoon-facing environments in any atoll-rim zone
480 through overwash and run-up processes. During strong cyclones, the water level in the open ocean like that in
481 the lagoon can rapidly rise several metres above pmsl, and thus, approaching waves come onshore at both rim
482 sides as rising turbulent surges loaded with bioclastic sandy grains. Owing to their respective form (subspheric
483 and disk-shaped), *Amphistegina* and *Marginopora* tests have low settling velocity and high hydrodynamic
484 stability, thereby able to experience grain size selection and to be moved by suspension far from their production
485 areas (Montaggioni and Venec-Peyré, 1993). However, the dominance of foraminiferal tests (locally, up to 80%)
486 over other bioclasts in the sedimentary sequences close to the lagoon margins may suggest that the relevant
487 material came mostly from lagoonal deposits in which foraminifera is known to represent locally about 20% of
488 the total sand fraction (Adjas, 1988). In this view, the extension of the inner shoreline towards the lagoon would

be chiefly driven by sediment supply from nearby lagoonal bottoms.

The island accretionary model presented herein refers to the "central core" model defined by Woodroffe et al. (1999) in which island accretion starts from depocentres (i.e. central cores) and extends both oceanwards and lagoonwards through time. This model is also in total agreement with **Dickinson**'s claim (2004), indicating that coral-reef island formation was promoted by gradual sea level fall. Similarly, the present scenario is closely linked to works by McLean and Woodroffe (1994), Richmond (1992), Woodroffe et al. (1999). These authors suggested the presence of hard basements close to or at sea level as a prerequisite for island formation. By contrast, in other tropical Indian and Pacific areas, differing models of low-lying, coral island development were described, in which main accretion occurred during marine transgressive to high-stand periods (Kench et al., 2005, 2014; East et al., 2018). In any case, long-term atoll-island stabilty would be governed by sea level changes. As formed in different sea-level contexts, i.e. transgressive, regressive or at higher than present, stabilized sea-level, islands will be going to respond differentially to the predicted sea-level rise. Those accreted during marine regressive events may be altered by rising sea levels, especially if sea level is expected to rise at rates up to 8 mm/yr (Botella, 2015), storminess to increase in intensity and vertical reef-growth rates to not exceed 4-5 mm/yr on average (Perry et al., 2018) in the next decades.

6. Conclusions

From chronostratigraphic analysis of seven excavations across two transects from the south-eastern, windward and south-western, leeward rim sides at Takapoto Atoll emerges a number of highlights relating to the history of atoll-island development in the north-western Tuamotu.

Storminess, especially cyclone activity, appears to be the major control of island formation, as demonstrated by textural and compositional patterns of the motus. Island stratigraphy is typified by a decreasing grain-size trend from the outer border lagoonwards. Gravel-dominated deposits grade laterally into gravelly, sand-supported to sand-dominated sediments as expressing a decreasing transport capacity of wave surges inwards. Dominant gravel components include pocilloporid corals, mostly derived from the adjacent, upper forereef zone. Sand-sized grains are prominently composed of foraminifera (amphisteginids, mainly), regarded as derived from open-sea environments and lagoonal bottoms as well. Distinct depositional sequences are composed of units, to 2 m thick at the windward, outer island margin, but not exceeding 0.40 m at other settings. Most sequences exhibit a fining-upward, graded bedding.

Based on 62 radiometric ages of skeletal material and preserved stratigraphic characteristics of the excavated deposits, the history of atoll-island development is reconstructed in relation to mid to late Holocene sea-level changes. The basal conglomerate pavements on which motus have settled began to form prior to about 2,600 yr BP over pre-existing reef flat surfaces as sea level was stabilized at about +0.80 m above pmsl. While deposition of conglomerates in the making occurred mainly during a period of high still-stand relative to present, the main phases of island development took place in a context of sea-level drop from about 2,300 yr BP to present. From about 1,500 yr BP, on both rim sides, islands started to growth from subcircular to elongate, partly emerging, patchily distributed depocentres (islets). They continued to spread out concentrically, reaching lagoon margins as soon as 1,000 yr BP. Over the last centuries, islets extended mainly oceanwards to form continuous islands. The dataset gives sufficient evidence to believe that this evolutionary scenario may be appropriate for explaining accretionary histories of other subsiding, northern Tuamotu atolls. However, this model would have to be tested in nearby atolls, especially those experiencing active uplifting, including Rangiroa, Tikehau, Mataiva and Tikehau Atolls (Montaggioni, 1985).

Dating of coral clasts revealed that, in the north Tuamotu, over the last 3,000 years, high-energy wave events occured at an average frequency of one to two per century with a recurrence time of 50 to 100 years. This puts in light the critical role of low-frequency, high-energy events in island shaping, especially in ocean-facing areas. However, a rapid rise in sea level could be an additional key factor in the future behaviour of atoll islands. Of great concern is how islands formed in a context of sea-level fall will respond to a sea-level predicted to regionally rise at rates of about 8 mm/yr in the next future, assuming rates of reef vertical accretion averaging 4–5 mm/yr and increasing cyclone intensity.

Acknowledgements

This work was supported by the French National 791 Research Agency (CNRS) under the STORISK research project (N° ANR-15-CE03-0003). Field work has benefited from logistical support and help from the research station of the Office of Marine Resources in Takapoto, Gaby Maiti Haumani. The authors warmly thank the following colleagues for their contributions: Norbert Faarii for engineering the excavation in the south eastern area of the atoll, Michel Pichon, Museum of Tropical Queensland, Townsville, for identification of coral samples. Thanks to the inhabitants of the atoll for having kindly transmitted their local knowledge. Excavations A, B, C and D are located on parcel A 510 of the land register (Terre Ohavana, owner Faarii Norbert Tetu

husband of Kaua Tevaha Tegahhe known as Denise). Excavations F and G are located on parcel A. 348 of the land register (Terre Orohoe, owner "successsion Teamanaha in Manake - F.O.). Excavation H is located on parcel A 356 of the land register (Owner French Polynesia, by default). Field work and sampling have been conducted from the end of February to early March 2018 by BS and AA. U/Th and AMS radiocarbon dating were performed by EPB and AD. AMS radiocarbon of Sample SAT 97A2 was performed by the French National facility Artemis LMC14 (LSCE (CNRS–CEA/UVSQ)-IRD-IRSN-MC) Saclay, France. The corresponding author, LFM, was in charge of interpretating the data and drafting the article in collaboration with allhis co-authors. BS and AA provided field pictures. Figures were conceived by LFM and BM-G.

Many thanks to Serge Planes and Bruno Delesalle for financially supporting a number of U/Th analyses. Our recognitions are extensive to Claudée Noury, Cédric Goulas, Louise Bordier, Lorna Foliot for contributing to sample preparation for U/Th analysis and Jean-Pascal Dumoulin for 14-C analysis. Marie-Thérèse Vénec-Peyré is warmly thanked for identification of foraminiferal tests. Many thanks to Reviewers C.D. Storlazzi and C.D. Woodroffe for their useful comments.

References

Adjas, A., 1988. Sédimentologie comparée de quelques modèles lagonaires actuels des milieux récifaux coralliens du Pacifique (Nouvelle Calédonie, Polynésie). Unpublished PhD. Thesis, Aix-Marseille Univ., 340 p.

Andersen M. B., Stirling C. H., Zimmermann B., Halliday A. N., 2010. Precise determination of the open ocean $^{234}U/^{238}U$ composition. Geochem. Geophys. Geosyst. 11: doi.org/10.1029/2010GC003318

Andréfoüet, S., Ardhuin, F., Queffeulou, P., Le Gendre, R., 2012. Island shadow effect and the wave climate of the Western Tuamotu Archipelago (French Polynesia) inferred from altimetry and numerical model data. Mar. Pollut. Bull. 65, 415–424.

Aslam, M., Kench, P.S. 2017. Reef island dynamics and mechanisms of change in Huvadhoo Atoll, Republic of Maldives, Indian Ocean. Anthropocene, 18, 57–68.

Bard, E., Hamelin, B., Arnold, M., Montaggioni, L.F., Cabioch, G., Faure, G., Rougerie, F., 1996. Deglacial sea-level record from Tahiti corals and the timing of global meltwater discharge. Nature 382, 241–244.

Becker, M., Meyssignac, B., Letetrel, C., Llovel, W., Cazenave, A., Delcroix, T., 2012. Sea level variations at tropical Pacific islands since 1950. Glob. Planet. Change 80-81, 85–98.

572 Beetham, E., Kench, P.S. 2018. Predicting wave overtopping thresholds on coral reef-island shorelines with
573 future sea-level rise. Nat. Commun. 9:3997 |DOI: 10.1038/s41467-018-06550-1

574 Bouchon, C., 1983. Les peuplements de scléractiniaires de l'atoll de Takapoto (Polynésie Française). J. Soc.
575 Océanistes 77, 35–42.

576 Bourrouilh-Le Jan, F.G., Talandier, J., 1985. Sédimentation et fracturation de haute énergie en milieu récifal:
577 tsunamis, ouragans et cyclones et leurs effets sur la sédimentologie et la géomorphologie d'un atoll: motu et hoa,
578 Rangiroa, Tuamotu, Pacifique SE. Mar. Geol. 67, 263–272.

579 Botella, A. 2015. Past and future sea level changes in French Polynesia. MSc. Thesis, University of Ottawa,
580 Canada, pp. 94.

581 Canavesio, R., 2014. Estimer les houles cycloniques à partir d'observations météorologiques limitées: exemple
582 de la submersion d'Anaa en 1906 aux Tuamotu (Polynésie Française). Vertigo, 14, doi:10.4000/vertigo.15375

583 Canavesio, R., Pons-Branchu, E., Chancerelle, Y., 2018. Limitations to U/Th dating of reef-platform carbonate
584 boulders produced by high-energy marine inundations in the Tuamotu Archipelago (French Polynesia). Coral
585 Reefs, 37, 1139–1155.

586 Cheng, H., Lawrence Edwards, R., Shen, C.-C., Polyak, V. J., Asmerom, Y., Woodhead, J. D., Hellstrom, J.,
587 Wang, Y., Kong, X., Spötl, C., Wang, X., Calvin Alexander, E., 2013. Improvements in ^{230}Th dating, ^{230}Th and
588 234U half-life values, and U–Th isotopic measurements by multi-collector inductively coupled plasma mass
589 spectrometry, Earth Planet. Sci. Lett., 371–372, 82–91.

590 Chevalier, J.P., Denizot, M., Ricard, M., Salvat, B., Sournia, A., Vasseur, P., 1979. Géomorphologie de l'atoll de
591 Takapoto. J. Soc. Océanistes, 62, 9–18.

592 Chivas, A., Chappell, J., Polach, H., Pillans, B., Flood, P., 1986. Radiocarbon evidence for the timing and rate of
593 island development, beach-rock formation and phosphatization at Lady Elliot Island, Queensland, Australia.
594 Mar.Geol. 69, 273–287.

595 Dickinson, W.R., 2004. Impacts of eustasy and hydro-isosasy on the evolution and landforms of Pacific atolls:
596 Palaeogeogr. Palaeoclimatol. Palaeoecol. 213, 251–269.

597 Dickinson, W.R., 2009.Pacific atoll living: how long already and until when. GSA Today 19, 4–10.

598 Dupon, J.-F., 1987. Les atolls et le risque cyclonique. Le cas des Tuamotu. Cah. Sci. Hum.23, 567–599.

599 Duvat, V.K.E., Salvat, B., Salmon, C., 2017. Drivers of shoreline change in atoll reef islands of the Tuamotu
600 Archipelago, French Polynesia. Glob. Planet. Change 158, 134–154.

601 East, H.K., Perry, C.T., Kench, P.S., Liang, Y., Gulliver, P., 2018. Coral reef island initiation and development
602 under higher than present sea levels. Geophys. Res. Lett. 45, 11,265–11,274.

603 Etienne, S., 2012. Marine inundation hazards in French Polynesia: geomorphic impacts of Tropical Cyclone Oli
604 in February 2010. In: Terry, J.P., Goff, J. (Eds), Natural Hazards in the Asia-Pacific region: Recent Advances
605 and Emerging Concepts. Geol. Soc. London, Spec. Publ., 361, pp. 21–39.

606 Hallmann, N., Camoin, G., Eisenhauer, A., Botella, A., Milne, G.A., Vella, C., Samankassou, E., Pothin, V.,
607 Dussouillez, P., Fleury, J., Fietzke, J., 2018. Ice volume and climate changes from a 6000 year sea-level record
608 in French Polynesia. Nat. Commun. 9. https://doi. org/10.1038/s41467-017-02695-7.

609 Harmelin-Vivien, M.L., 1994. The effects of storms and cyclones on coral reefs: a review. J. Coast. Res. Spec.
610 Issue 12, Coastal Hazards, 211–231.

611 Harmelin-Vivien, M.L., Laboute, P., 1986. Catastrophic impact of hurricanes on atoll outer reef slopes in the
612 Tuamotu (French Polynesia). Coral Reefs 5, 55–62.

613 Hayne, M., Chappell, J., 2001. Cyclone frequency during the last 5000 years at Curacoa Island, north
614 Queensland, Australia. Palaeogeogr. Palaeoclimatol. Palaecol. 168, 207–219.

615 Jaffey, A.H., Flynn, K.F., Glendenin, L.E., Bentley, W.C., Essling, A.M., 1971. Precision measurements of half-
616 lives and specific activities of ^{235}U and ^{238}U. Phys. Rev. C, 4, 1889–1906.

617 Kench, P.S., McLean, R.F., Nichol, S.L., 2005. New model of reef-island evolution: Maldives, Indian Ocean.
618 Geology 33, 145–148.

619 Kench, P.S., Owen, S.D., Ford, M.R., 2014. Evidence for coral island formation during rising sea level in the
620 central Pacific Ocean. Geophys. Res. Lett. 41, 820–827.

621 Kench, P.S., Thompson, D., Ford, M.R., Ogawa, H., McLean, R.F. 2015. Coral reef islands defy sea-level rise
622 over the past century: records from a central Pacific atoll. Geology, 43, 515–518.

623 Kench, P.S., Ford, M.R., Owen, S.D. 2018. Patterns of island change and persistence offer alternate adaptation
624 pathways for atoll nations. Nat.Commun. 9, 605.

625 Kühlmann, H.H., Chevalier, J.-P., 1986. Les coraux (scléractiniaires et hydro-coralliaires) de l'atoll de Takapoto,
626 îles Tuamotu: aspects écologiques. Mar. Ecol. 7, 75–104.

627 Laboute, P., 1985. Evaluation des dégats causés par les passages des cyclones de 1982-1983 en Polynésie
628 Française sur les pentes externes des atolls de Tikehau et de Takapoto (Archipel des Tuamotu). Proc. Fifth
629 Intern. Coral Reef Congr. 3, 323–329.

630 Larrue, S., Chiron, Th., 2010. Les îles de Polynésie Française face à l'aléa cyclonique. Vertigo, 10, DOI:
631 10.4000/vertigo.10558

632 Lau, A.Y.A., Terry, J.P., Switzer, A.D., Lee, Y., Etienne, S., 2016. Understanding the history of extreme wave
633 events in the Tuamotu Archipelago of French Polynesia from large carbonate boulders on Makemo Atoll, with
634 implications for future threats in the central South Pacific. Mar. Geol. 380, 174–190.

635 Laurent, V., Varney, P., 2014. Histoire des cyclones de Polynésie Française de 1831 à 2010. Météo-France,
636 ISBN 978-2-9522946-1-4, 172 pp.

637 McLean, R. F., Woodroffe, C.D., 1994. Coral atolls. In: Carter, R.W.G. and Woodroffe, C.D., (Eds.). Coastal
638 evolution: Late Quaternary Shoreline Morphodynamics. Cambridge Univ. Press, Cambridge, United Kingdom,
639 pp. 267–302.

640 Montaggioni, L.F., 1985. Makatea Island, Tuamotu Archipelago. Proc. Intern. Coral Reef Congr. 1, 103–158.

641 Montaggioni, L.F., 2005. History of Indo-Pacific coral reef systems since the last deglaciation: development
642 patterns and controlling factors. Earth Sci. Rev. 71, 1–75.

643 Montaggioni, L.F., Pirazzoli, P.A., 1984. The significance of exposed coral conglomerates from French
644 Polynesia (Pacific Ocean) as indicators of recent relative sea-level changes. Coral Reefs 3, 29–42.

645 Montaggioni, L.F., Vénec-Peyré, M.-Th., 1993. Shallow-water foraminiferal taphocoenoses at Site 821:
646 implications for the Pleistocene evolution of the central Great Barrier Reef shelf, Northeastern Australia. Proc.
647 Ocean Drilling Program, Sc. Res. 133, 365–378.

Montaggioni, L.F., Salvat, B., Aubanel, A., Eisenhauer, A., Martin-Garin, B. 2018. The mode and timing of windward reef-island accretion in relation with Holocene sea-level change: a case study from Takapoto Atoll, French Polynesia. Geomorphology, 318, 320–335.

Montaggioni, L.F.*, Collin, A., James, D., Salvat, B., Martin-Garin, B., Siu, G., Taiarui, M., Chancerelle, Y. 2019. Morphology of fore-reef slopes and terraces, Takapoto Atoll (Tuamotu Archipelago, French Polynesia, central Pacific): the tectonic, sea-level and coral-growth control. Mar.Geol. 417, 106027.

Nunn, P.D., 2007. Climate, Environment and Society in the Pacific during the Last Millennium. Develop. Earth Envir. Sci, 6, Elsevier, Amsterdam, the Netherlands, 316 pp.

Nurse, L.A., McLean, R.L., Agard, J., Briguglio, L.P., Duvat-Magnan,V., Pelesikoti, N., Tompkins, E., Webb, A., 2014. Small islands. In: Barros, V.R., Field, C.B., Dokken, D.J., Mastrandrea, K.J. Mach, M.D., Bilir, T.E., Chatterjee, M., Ebi, K.L., Estrada, Y.O., Genova, R.C., Girma, B., Kissel, E.S., Levy, A.N., MacCracken, S., Mastrandrea, P.R., andWhite, L.L. (Eds.). Climate Change 2014: Impacts, Adaptation, and Vulnerability. Part B: Regional Aspects. Contribution of Working Group II to the Fifth Assessment Report of the Intergovernmental Panel on Climate Change. Cambridge University Press, Cambridge, United Kingdom and New York, NY, USA, pp. 1613–1654.

Perry, C.T., Kench, P.S., Smithers, S.G., Riegl, B., Yamano, H., O'Leary, M.J., 2011. Implications of reef ecosystem change for the stability and maintenance of coral reef islands. Glob. Change Biol. 17, 3679–3696.

Perry et al., 2018. Loss of coral reef growth capacity to track future increases in sea level. Nature, doi.org/10.1038/s41586-018-0194-z.

Pirazzoli, P.A., Montaggioni, L.F., 1986. Late Holocene sea-level changes in the northwest Tuamotu Islands, French Polynesia. Quat. Res. 25, 350–368.

Pirazzoli, P.A., Montaggioni, L.F., 1988. Late Holocene sea-level changes in French Polynesia. Palaeogeogr. Palaeoclimatol. Palaeoecol. 68, 153–175.

Pons-Branchu E, Douville E, Dumont E, Branchu P, Thil F, Frank N. , Bordier L and Borst W., 2014. Cross-dating (U/Th and lamina counting) of modern carbonate deposits in underground Paris, France. A new archive for urban history reconstructions: case study of anthropic Rare Earth and Yttrium release. Quat. Geochronol. 24, 44–53.

675 Presto, M.K., Ogston, A.S., Storlazzi, C.D., Field, M.E., 2006. Temporal and spatial variability in the flow and
676 dispersal of suspended sediment on a fringing reef flat, Molokai, Hawaii. Estuar.Coast. Shelf Sc. 67, 67–81.

677 Reimer, P.J., Bard, E., Bayliss, A., Beck, J.W., Blackwell, P.G., Bronk Ramsey, Ch., Buck, C.E., Cheng, H.,
678 Edwards, R.L., Friedrich, M., Grootes, P.M., Guilderson, T.P., Haflidason, H., Hadjas, I., Hatté, Ch., Heaton,
679 T.J., Hoffmann, D.L., Hogg, A.G., Hughen, K.A., Kaiser, K.F., Kromer, B., Manning, S.W., Niu, M., Reimer,
680 R.W., Richards, D.A., Scott, E.M., Southon, J.R., Staff, R.A., Turney, Ch. S.M., van der Plicht, J., 2013.
681 Intercal13 and marine13 radiocarbon age calibration curves 0-50,000 years Cal. Radiocarbon 55, 1869–1887.

682 Richmond, B.M., 1992. Development of atoll islets in the central Pacific. Proc. Seventh Int. Coral Reef Symp. 2,
683 1185–1194.

684 Salvat, B., 1981. Geomorphology and marine ecology of the Takapoto Atoll (Tuamotu Archipelago). Proc.
685 Fourth Intern. Coral Reef Symp., Manila, 1, 503–509.

686 Salvat, B., Richard, G., 1985. Takapoto Atoll, Tuamotu Archipelago. Proc. Intern. Coral Reef Congr. 1, 323–
687 378.

688 Sladen, A., Hébert, H., Schindelé, F., Reymond, D., 2007. Evaluation of far-field tsunami hazard in French
689 Polynesia based on historical and numerical simulations. Nat. Hazards Earth Syst. Sci. 7, 195–206.

690 Storlazzi, C. D, Elias, E.P.L., Berkowitz, P., 2015. Many atolls may be uninhabitable within decades due to
691 climate change. Sci. Rep. 5, 14546; doi: 10.1038/srep14546.

692 Storlazzi, C.D., Gingerich, S.B., van Dongeren, A., Cheriton, O.M., Swarzenski, P.W., Quataert, E., Voss, C.I.,
693 Field D.W., Annamalai, H., Piniak G.A., McCall, R., 2018. Most atolls will be uninhabitable by the mid-21st
694 century because of sea-level rise exacerbating wave-driven flooding. Science Advances, 4, eaap9741, DOI:
695 10.1126/sciadv.aap9741

696 Terry, J.P., Goff, J., 2014. Megaclasts: proposed revised nomenclature at the coarse end of the Udden-
697 Wentworth grain-size scale for sedimentary particles. J. Sedim. Res. 84, 192–197.

698 Toomey, M.R., Donnelly, J.P., Woodruff, J.D., 2013. Reconstructing mid-late Holocene cyclone variability in
699 the central Pacific using sedimentary record from Tahaa, French Polynesia. Quat. Sci. Rev. 77, 181–189.

Woodroffe, C.D., McLean, R.F., Smithers, S.G., Lawson, E.M., 1999. Atoll reef-island formation and response to sea-level change: West Island, Cocos (Keeling) Islands. Mar. Geol. 160, 85–104.

Woodroffe, C.D., Samosorn, B., Hua, Q., Hart, D.E., 2007. Incremental accretion of a sandy reef island over the past 3000 years indicated by component-specific radiocarbon dating. Geophys. Res. Lett. 34, L03602, doi:10.1029/2006GL028875

Yu, K., Zhao, J., Roff, G., Lybolt, M., Feng, Y., Clark, T., Li, S., 2012. High-precision U-series ages of transported coral blocks on Heron reef (southern Great Barrier Reef) and storm activity during the past centuries. Palaeogeogr. Palaeclimatol. Palaeoecol. 337–338, 23–36.

Table and Figure captions

Table 1. Uranium/Thorium data of coral samples from Takapoto Atoll. Are given successively laboratory sample codes, field sample (SAT) numbers, uranium and thorium contents, isotopic composition with statistical errors (two standard deviations of the mean) and ages. $\delta^{234}U_m = (\{^{234}U/^{238}U\}_{measured}/\{^{234}U/^{238}U\}_{equilibrium} - 1) \times 1000$, with $^{234}U/^{238}U_{equilibrium} = 54.89\times10^{-6}$ (molar ratio. Cheng et al.. 2013). $\delta^{234}Ui$ is the $\delta^{234}U$ at initial time (using U/Th ages). Ages are expressed in years BP (Before Present), relative to the year of sample analysis (2019 for samples from 7813 and 2018 from the other samples) and are corrected for detrital content using a $^{230}Th/^{232}Th$ isotopic ratio = .7 ± 50%.For sample Exc. B - SAT 55 B, “e” is for external part and “I” is for internal part.

Table 2. Selection of dated coral samples, younger than 2,000 yr BP, with ages expressed in calendar years of the commun era (CE).

Fig. 1. A) Location map of Takapoto Atoll in the Tuamotu Archipelago (French Polynesia, central Pacific). B) Te Fenua map of Takapoto Atoll showing location of the two studied areas, labelled as SE (south-east) and SW (south-west). C–D) Aerial views of both rim sides of Takapoto Atoll, showing location of the seven excavation sites from the SE and SW profiles respectively: south-eastern (see Figure 2) and south-western (see Figure 3) profiles.

Fig. 2. South-eastern, windward profile, with location and lithostratigraphy of excavations A, B, C, and E (see Figs. 9, 10 and 11 for close-up views). Are also given location and radiometric age of coral samples (SAT) collected within each excavation – see Table 1 for details of dates. Ages are expressed in years BP.

Fig. 3. South-western, leeward profile, with location and lithostratigraphy of excavations F, G and H (see Figs. 8, 9, 10 and 11 for close-up views). Are also given location and radiometric age of coral samples (SAT) collected within each excavation – see Table 1 for details of dates. Ages are expressed in years BP.

Fig. 4. Plot of U/Th dated coral samples versus their respective stratigraphic location at the south-eastern, windward excavation sites (see Figs. 1C and 2 for sample location). Ages are expressed in years BP. Note trends in decreasing ages from base to top. The numbers refer to field SAT samples (see Table 1 for details of dates).

Fig. 5. Plot of U/Th dated coral samples versus their respective stratigraphic location at the south-western, leeward excavation sites (see Fig. 1D and 3 for sample location). Ages are expressed in years BP. Note trends in decreasing ages from base to top. The numbers refer to field SAT samples (see Table 1 for details of dates).

Fig. 6. Cross-section of the south-eastern, windward rim profile, with location of excavations A, B, C, and E. The numbers within each excavation refer to ages of the dated samples as positioned according to their stratigraphic level. Elevations are given relative to surfaces of the underlying conglomerate platforms. The dashed lines relate to accretion isochrons (years BP) based on the dated intervals within excavations. WT: water table level.

Fig. 7. Cross-section of the south-western, leeward rim profile, with location of excavations F, G and H. The numbers within each excavation refer to ages of the dated samples as positioned according to their stratigraphic level. Elevations are given relative to surfaces of the underlying conglomerate platforms.The dashed lines relate to accretion isochrons (years BP) based on the dated intervals within excavations. WT: water table level.

Fig. 8. Views of the stratigraphic sequences from both windward and leeward excavations. A) Excavation B (windward side): the uppermost 0.50 m are of gravel-supported facies while the 1 m-thick, lower section is composed of sand-supported, gravels. The cavity floor with the label is the top surface of the underlying conglomerate platform. B) Excavation C (windward side): the sequence is overtopped by a 0.25 m-thick, organic-rich unit. To depth of 0.60 m, sand is dominating. Below, the facies is sand-supported, gravelly. The conglomeratic floor is drowned under the water table. C) Excavation E (windward side): an about, 0.30 m-thick,

751 organic-rich layer caps the sequence (1.50 m in total thickness). Sediments are sand-dominated. The
752 conglomeratic basement is inundated. D) Excavation G (leeward side): below the gravelly top surface and a
753 0.50 m-thick, organic-rich unit, appears a bed, about 0.90 m-thick, composed prominently of foraminifera-rich
754 sands. The basal conglomerate pavement is flooded by the water table.

755 **Fig. 9.** Gravel-dominated facies from both windward and leeward rim sites. The stick is decimetre-calibrated. A)
756 Close-up of Excavation B (windward side), showing the stratigraphic sequence from top to 1.10 m deep. The top
757 0.40 m bed is gravel-supported, while the lower 0.80 m layer is of sand-supported, gravel facies. B) Close-up of
758 Excavation F (leeward side), showing the uppermost section (0.60 m-thick) composed of sand-supported gravels.
759 The lower 0.10 m-thick layer is of gravel-supported facies. C) Close-up of Excavation F (leeward side), showing
760 the section from 1.0 to 2.0 m below top surface. It exibits three superimposed, fining-upward, gravel-supported
761 units, ranging each from 0.30 to 0.40 m in thickness. D) Close-up of Excavation A (windward side), showing
762 successively from top downhole: a 0.10 m-thick, organic-rich layer, a 0.30 m-thick gravel-supported unit, and a
763 sand-supported, gravel unit.

764 **Fig. 10.** Sand-dominated facies from both windward and leeward rim sites.

765 The stick is decimetre-calibrated. A) Close-up of Excavation C (windward side), showing sand-dominated facies
766 at depths of 0.83 to 1.20 m beneath top surface of the sequence. Locally, just below the sick, the sediment is
767 partly lithified as a caliche crust. B) Close-up of Excavation G (leeward side), showing a sand-dominated bed
768 overtopped by a brown-coloured, organic-and root-rich layer, about 0.50 m in thickness. The top surface of the
769 section is covered by gravel-dominated horizon. C) Close-up of Excavation H (leeward side) showing a sand-
770 dominated section, enriched in organic matter at its upper 0.25 m portion. D) Close-up of Excavation E
771 (windward side), showing alternations of foraminifera-rich and coralgal laminations, ranging between 10 and
772 20 mm in thickness.

773 **Fig. 11.** Organic-rich, sandy facies. Close-up of Excavation H (leeward side), showing an about 0.25 m-thick,
774 black-coloured, organic-rich bed, capping a sand-graded unit. The stick is decimetre-calibrated.

775 **Fig. 12.** Planimetric reconstruction of the south-eastern, windward atoll rim, showing successive island-accretion
776 phases over the past 1,500 years. Isochrons delineate the changing aerial extent of islets through time, from
777 1,500 yr BP to present. Initial depocentres are contained within the 2,000 yr-BP time-line clusters. Between
778 adjacent depocentres, prior to be infilled, spaces are believed to have been first bare of significant detrital

779 volumes and thus to have served as channels of water exchange between the open ocean and the lagoon, similar
780 to modern hoas. Islets extended to lagoon margins as soon as 1,000 yr BP, while they approached the modern
781 ocean-facing shoreline not prior to about 500 yr BP.

782 **Fig. 13.** Age distribution of identified wave-surge events throughout the last 2,000 years, based on U/Th dating
783 of coral gravels. For both windward and leeward rim sides, the blue dots refer to deposition of sand-dominated
784 samples, inner island areas; the red dots refer to deposition of gravel-dominated samples, outer island areas. The
785 ages of events identified herein are compared with those respectively reported by Lau et al., 2016 (crosses) and
786 Canavesio et al., 2018 (open circles) for the same time span.

787 **Fig. 14.** Conceptual evolutionary model of rim-island development at Takapoto Atoll. A) At around 7,000 yr BP,
788 as sea level was approximately −10 m below present mean sea level (pmsl), the reef pile of late Pleistocene age
789 culminated close to sea level. Coral communities started to colonize newly available substrates, while wave-
790 surge events began to move coral fragments upslope to reef top. B) From 6,000 to 5,000 yr BP, while sea level
791 rose to an elevation of about +0.80 m to +1.00 m above pmsl, the reef pile developed upwards, resulting in
792 deposition of a 4–5 m-thick, mid-Holocene unit, but remained still submerged at depths of −5 m to −6 m relative
793 to pmsl. The reef-rim top caught up with sea level during the late Holocene, by approximately 3000 yr BP. From
794 5,000 to 3,000 yr BP, sea level dropped by 0.10 m. Correlatively, reef aggradation continued to operate and to
795 deposit a few metre-thick, late Holocene unit. C) From 3,000 to 1,500 yr BP, sea level continued to fall down.
796 Coral clasts extracted from proximal upper reef slopes were deposited across the reef-rim areas and along the
797 lagoonal slopes. These deposits were the nuclei of basal conglomerate platforms. D) From 1,500 to 1,000 yr BP,
798 sea level dropped regularly toward its present position promoting cementation of conglomeratic basements.
799 Correlatively, coral gravels continued to accumulate over conglomerate beds, forming depocentres. These
800 extended laterally, predominently lagoonwards, forming discontinuous islets. E) From 1,000 to 500 yr BP, islets
801 develop dominantly oceanwards to finally form almost continuous islands. F) The present configuration of the
802 atoll island was acquired over the last centuries.

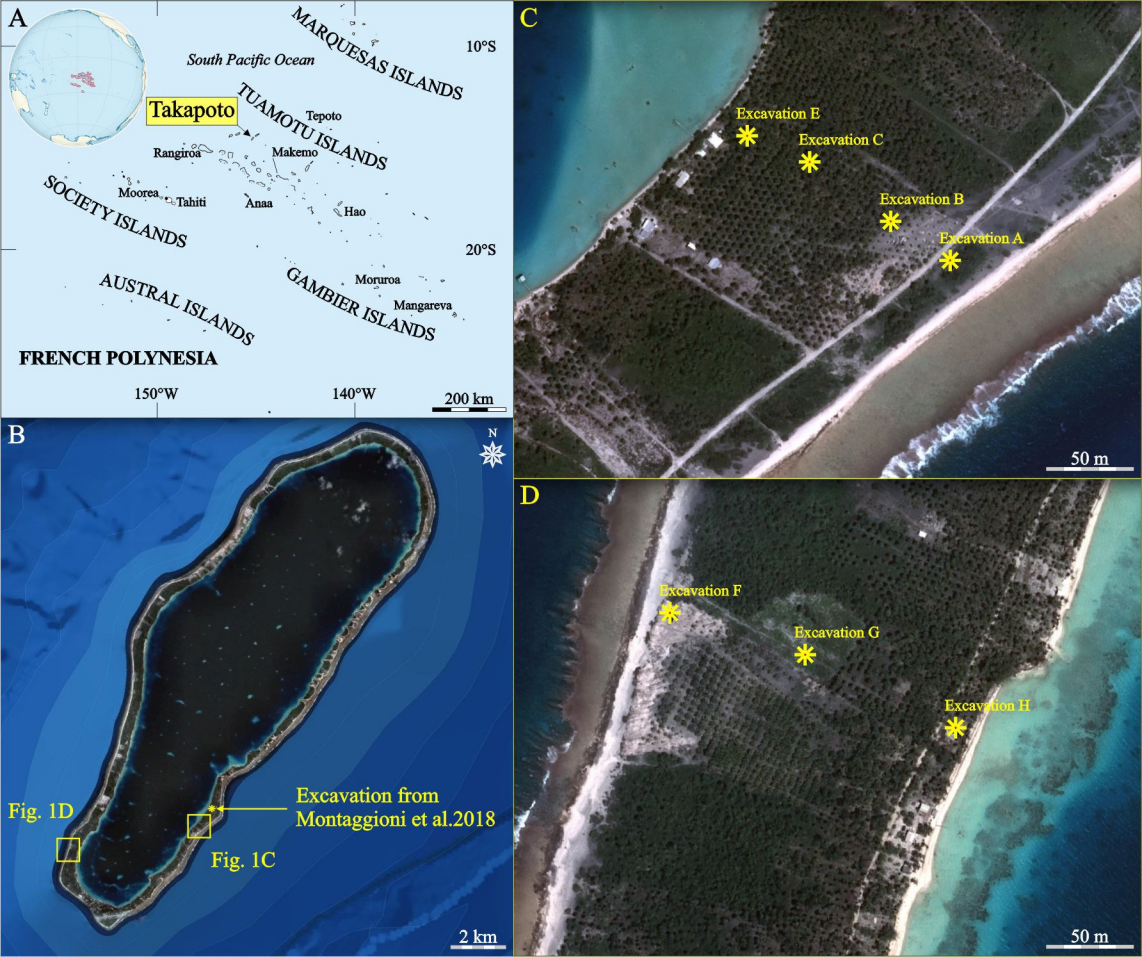
A
MARQUESAS ISLANDS
10°S
South Pacific Ocean
Takapoto
TUAMOTU ISLANDS
Tepoto
Rangiroa
Makemo
SOCIETY ISLANDS
Moorea
Tahiti
Anaa
Hao
20°S
AUSTRAL ISLANDS
GAMBIER ISLANDS
Mororuoa
Mangareva
FRENCH POLYNESIA
150°W
140°W
200 km
B
N
Fig. 1D
Excavation from Montaggioni et al.2018
Fig. 1C
2 km
C
Excavation E
Excavation C
Excavation B
Excavation A
50 m
D
Excavation F
Excavation G
Excavation H
50 m

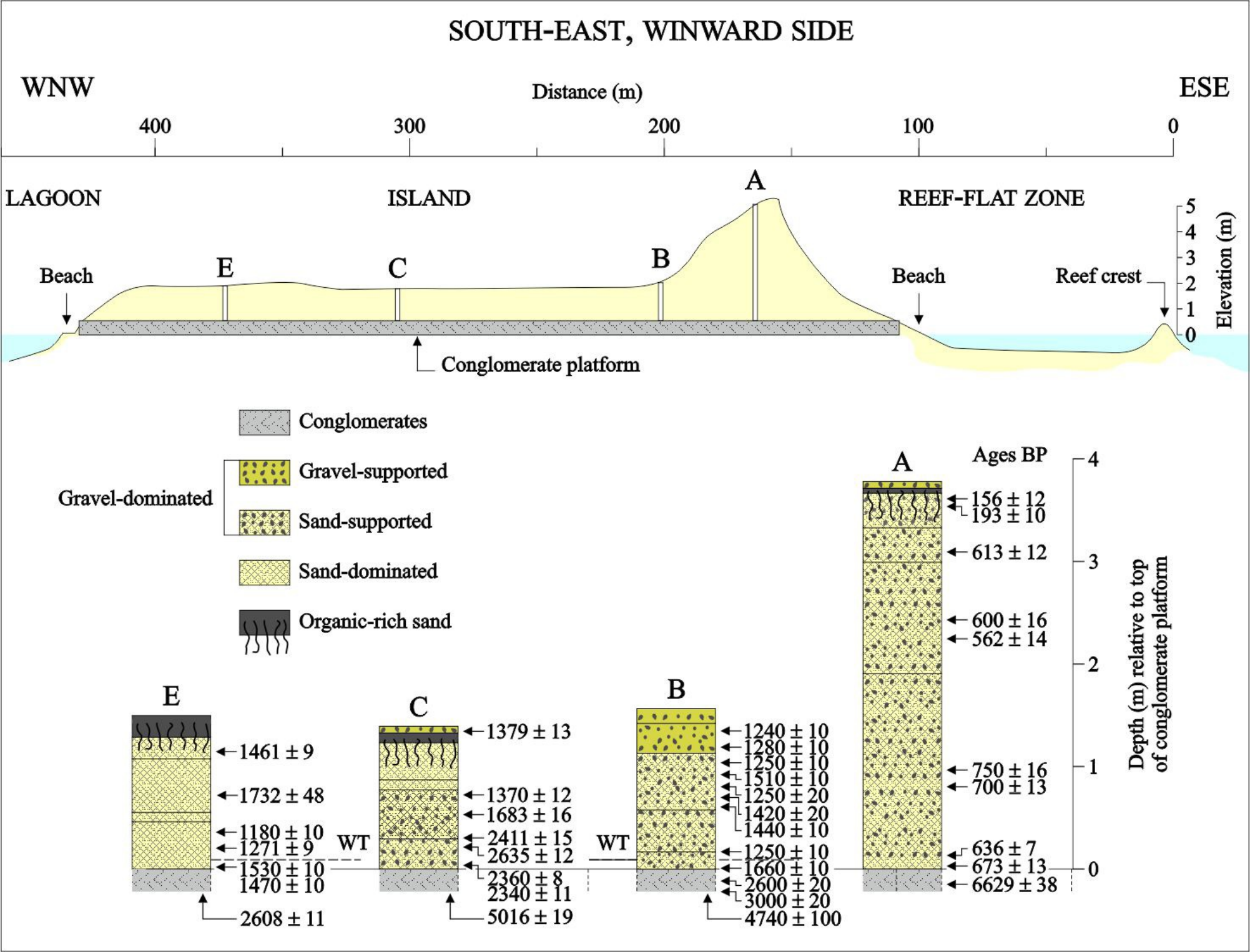
SOUTH-EAST, WINWARD SIDE
WNW
Distance (m)
ESE
400
300
200
100
0
LAGOON
ISLAND
REEF-FLAT ZONE
A
B
C
E
Beach
Beach
Reef crest
Elevation (m)
5
4
3
2
1
0
Conglomerate platform
Conglomerates
Gravel-dominated
Gravel-supported
Sand-supported
Sand-dominated
Organic-rich sand
Ages BP
Depth (m) relative to top of conglomerate platform
4
3
2
1
0
WT
WT
1461 ± 9
1732 ± 48
1180 ± 10
1271 ± 9
1530 ± 10
1470 ± 10
2608 ± 11
1379 ± 13
1370 ± 12
1683 ± 16
2411 ± 15
2635 ± 12
2360 ± 8
2340 ± 11
5016 ± 19
1240 ± 10
1280 ± 10
1250 ± 10
1510 ± 10
1250 ± 20
1420 ± 20
1440 ± 10
1250 ± 10
1660 ± 10
2600 ± 20
3000 ± 20
4740 ± 100
156 ± 12
193 ± 10
613 ± 12
600 ± 16
562 ± 14
750 ± 16
700 ± 13
636 ± 7
673 ± 13
6629 ± 38

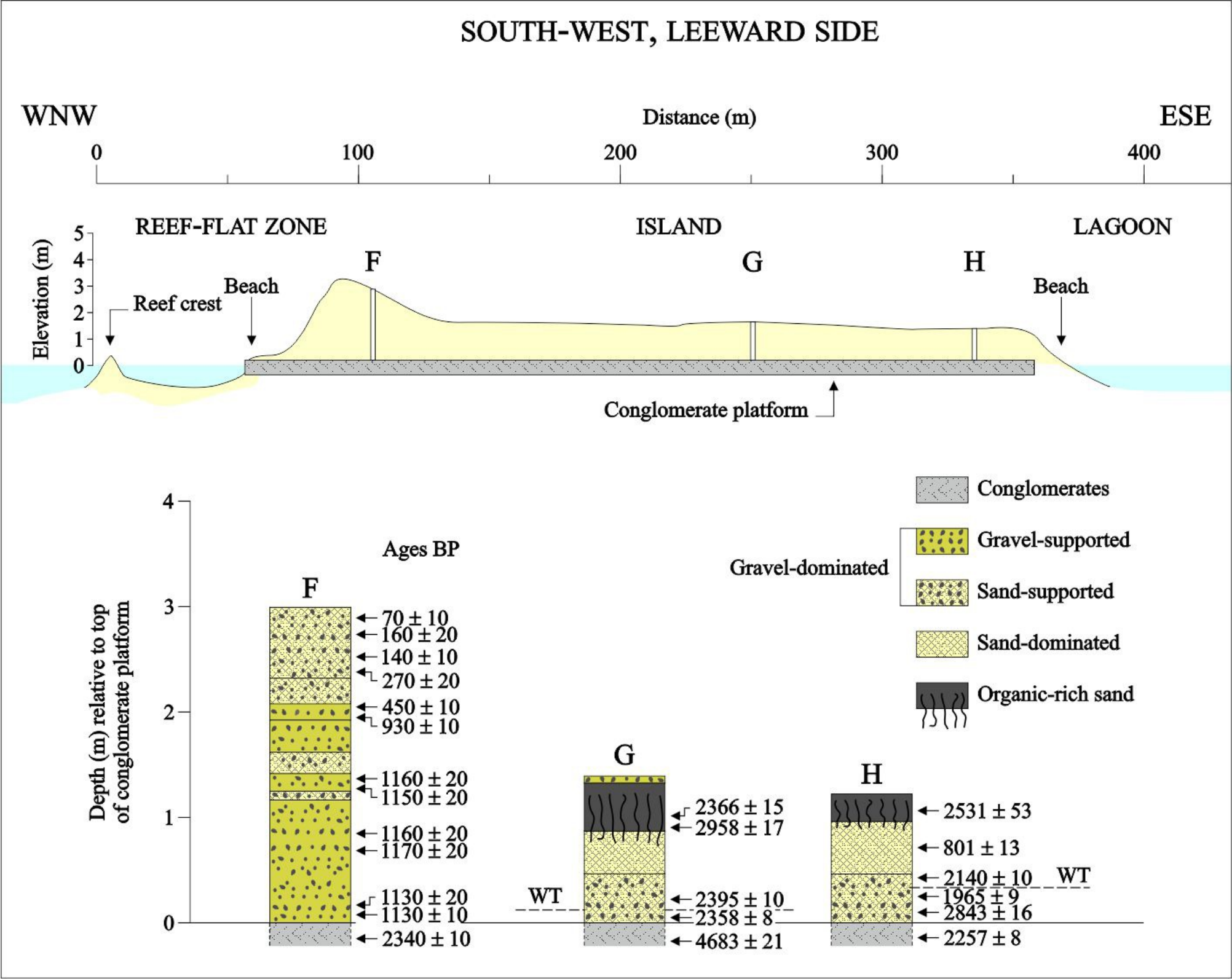
SOUTH-WEST, LEEWARD SIDE
WNW
Distance (m)
ESE
0
100
200
300
400
REEF-FLAT ZONE
ISLAND
LAGOON
Elevation (m)
5
4
3
2
1
0
F
G
H
Reef crest
Beach
Beach
Conglomerate platform
Depth (m) relative to top of conglomerate platform
4
3
2
1
0
Ages BP
F
70 ± 10
160 ± 20
140 ± 10
270 ± 20
450 ± 10
930 ± 10
1160 ± 20
1150 ± 20
1160 ± 20
1170 ± 20
1130 ± 20
1130 ± 10
2340 ± 10
G
2366 ± 15
2958 ± 17
WT
2395 ± 10
2358 ± 8
4683 ± 21
H
2531 ± 53
801 ± 13
2140 ± 10
WT
1965 ± 9
2843 ± 16
2257 ± 8
Gravel-dominated
Conglomerates
Gravel-supported
Sand-supported
Sand-dominated
Organic-rich sand

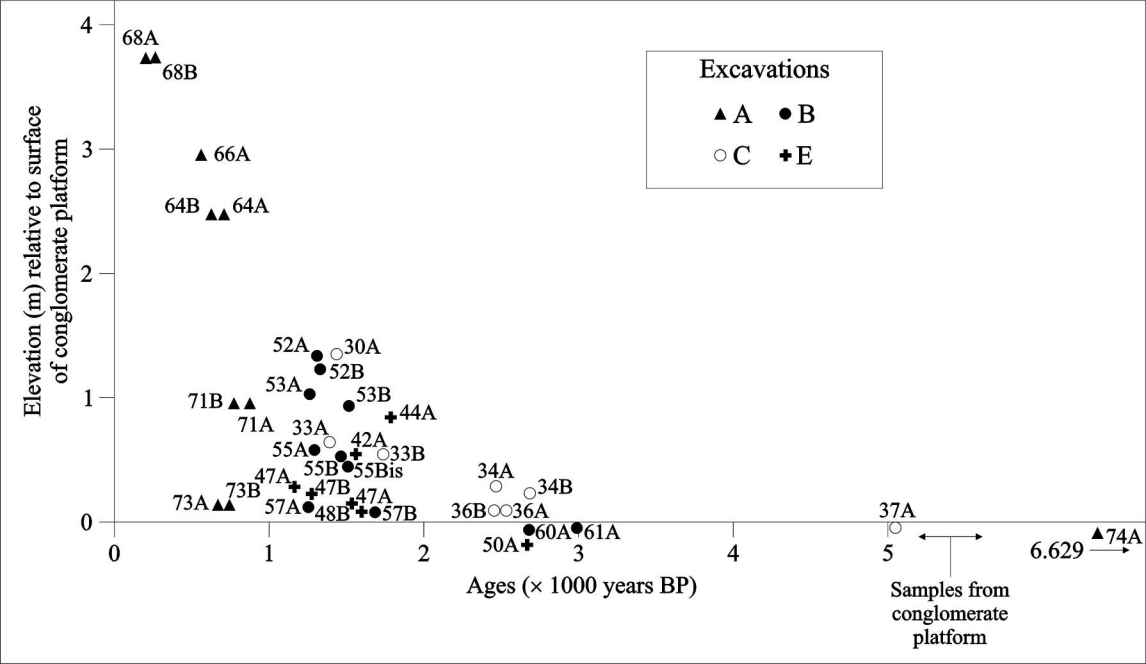
Elevation (m) relative to surface of conglomerate platform
Ages (× 1000 years BP)
Excavations
A
B
C
E
Samples from conglomerate platform
68A
68B
66A
64B
64A
52A
30A
52B
53A
53B
71B
71A
44A
33A
42A
55A
33B
55B
55Bis
34A
47A
73B
47B
34B
73A
57A
47A
48B
57B
36B
36A
37A
50A
60A
61A
74A
6.629
0
1
2
3
4
5

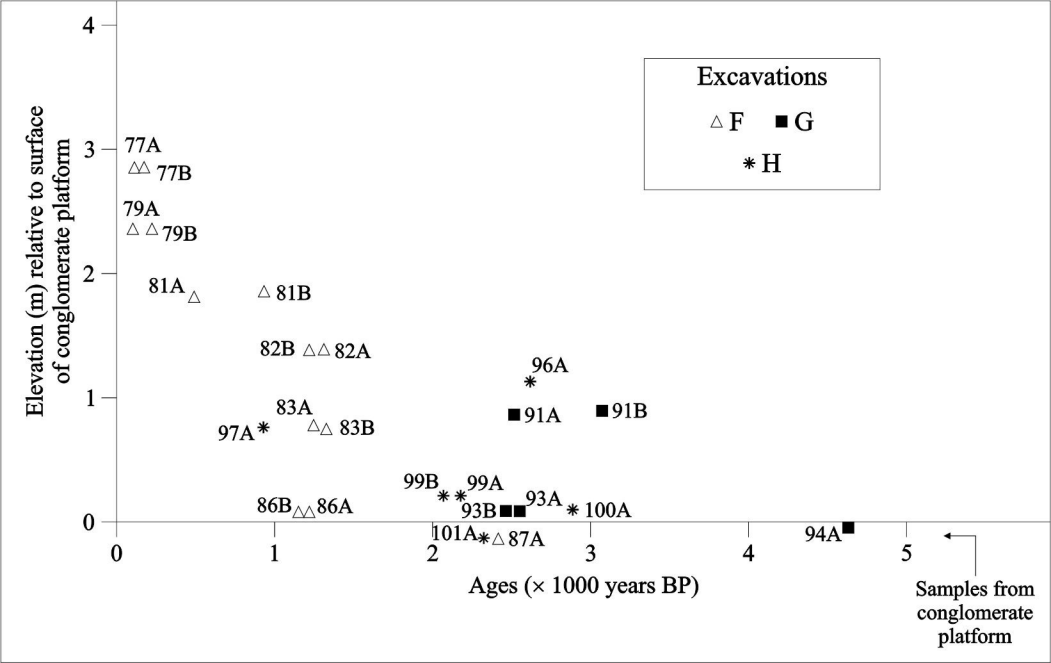
Excavations
F
G
H
Elevation (m) relative to surface of conglomerate platform
Ages (× 1000 years BP)
Samples from conglomerate platform
77A
77B
79A
79B
81A
81B
82B
82A
96A
83A
97A
91A
91B
83B
99B
99A
86B
86A
93B
93A
100A
101A
87A
94A
0
1
2
3
4
5

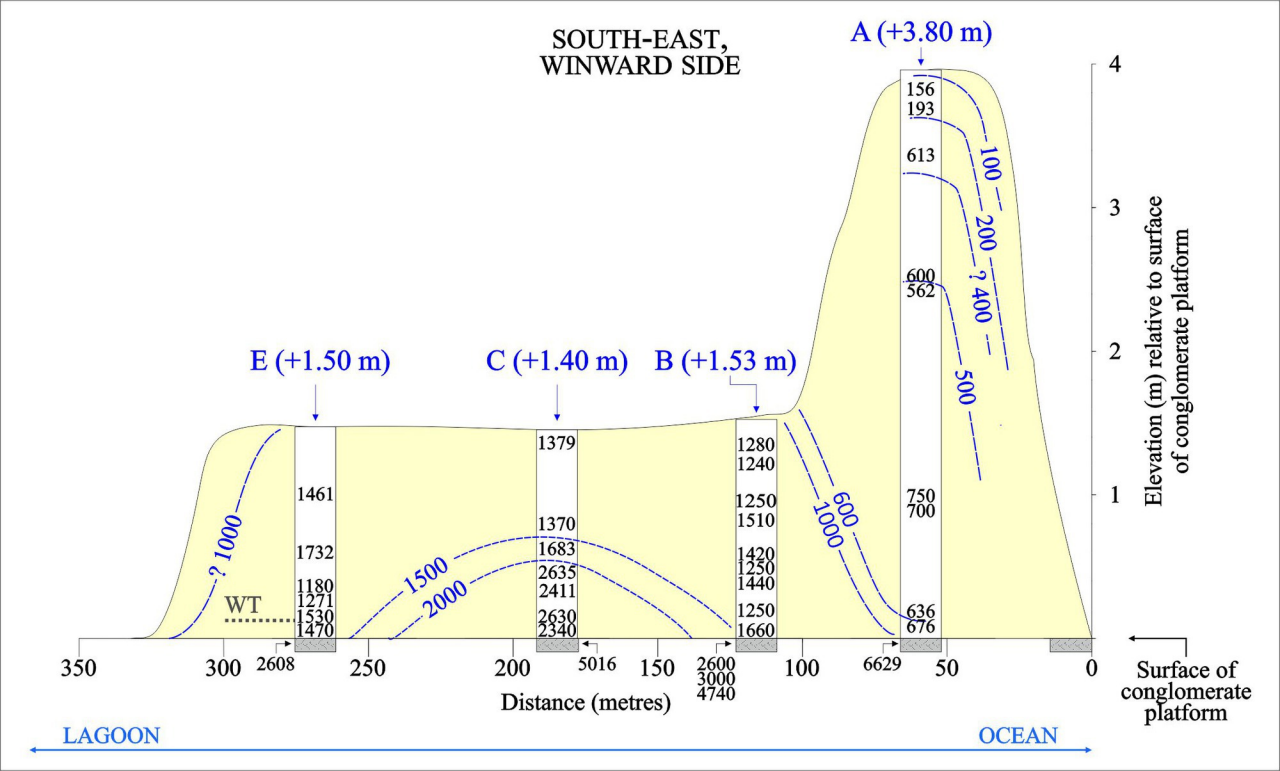
SOUTH-EAST,
WINWARD SIDE
A (+3.80 m)
E (+1.50 m)
C (+1.40 m)
B (+1.53 m)
156
193
613
600
562
750
700
636
676
100
200
? 400
500
600
1000
1461
1732
1180
1271
1530
1470
? 1000
WT
1379
1370
1683
2635
2411
2630
2340
1500
2000
1280
1240
1250
1510
1420
1250
1440
1250
1660
2608
5016
2600
3000
4740
6629
350
300
250
200
150
100
50
0
4
3
2
1
Elevation (m) relative to surface of conglomerate platform
Distance (metres)
Surface of conglomerate platform
LAGOON
OCEAN

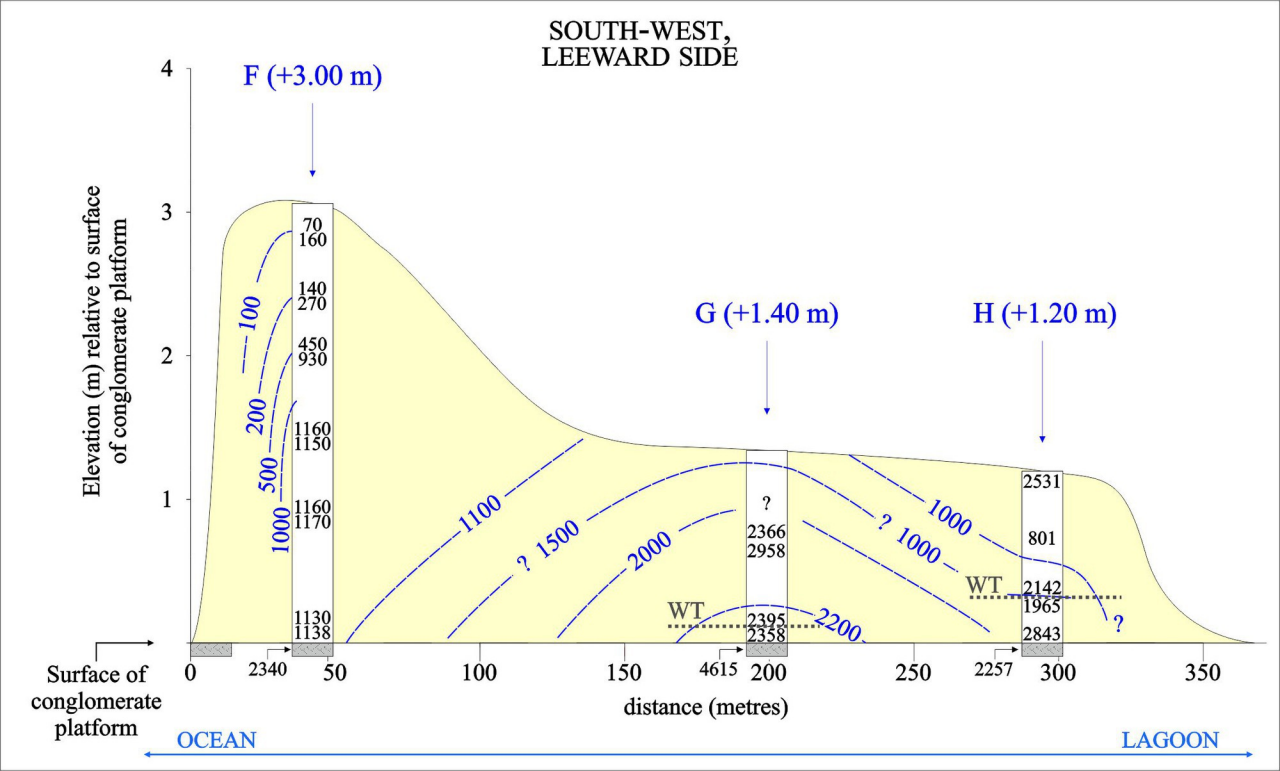
SOUTH-WEST,
LEEWARD SIDE
F (+3.00 m)
G (+1.40 m)
H (+1.20 m)
Elevation (m) relative to surface of conglomerate platform
4
3
2
1
100
200
500
1000
1100
? 1500
2000
? 1000
1000
70
160
140
270
450
930
1160
1150
1160
1170
1130
1138
?
2366
2958
2395
2358
2531
801
WT
2142
1965
2843
WT
2200
?
Surface of conglomerate platform
0
2340
50
100
150
4615
200
250
2257
300
350
distance (metres)
OCEAN
LAGOON

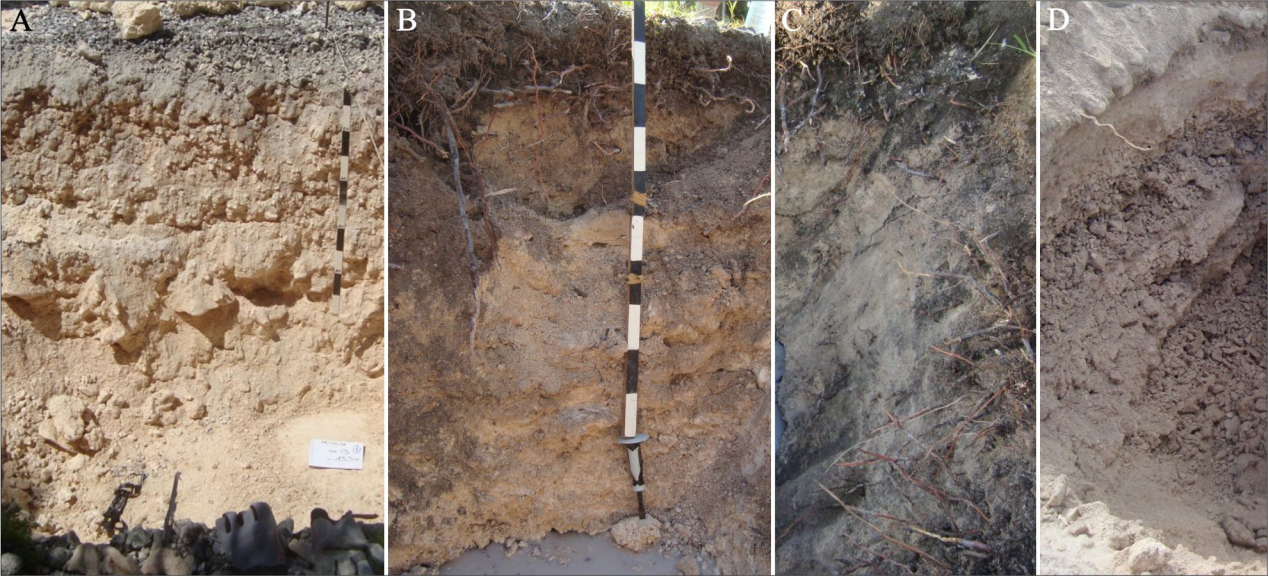
A
B
C
D


A
B
C
D
20
40
60
80
100


A


B

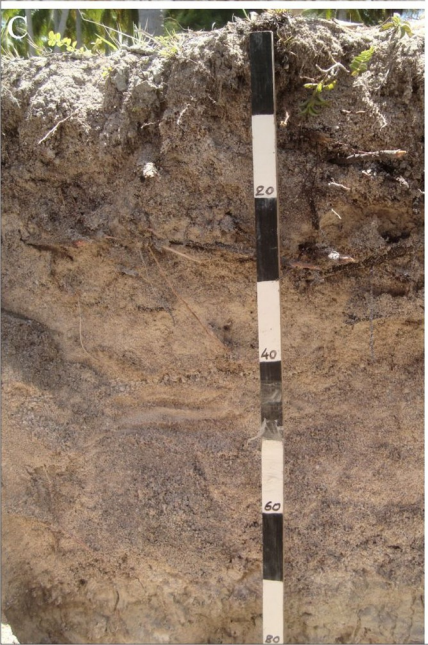
C
20
40
60
80


D

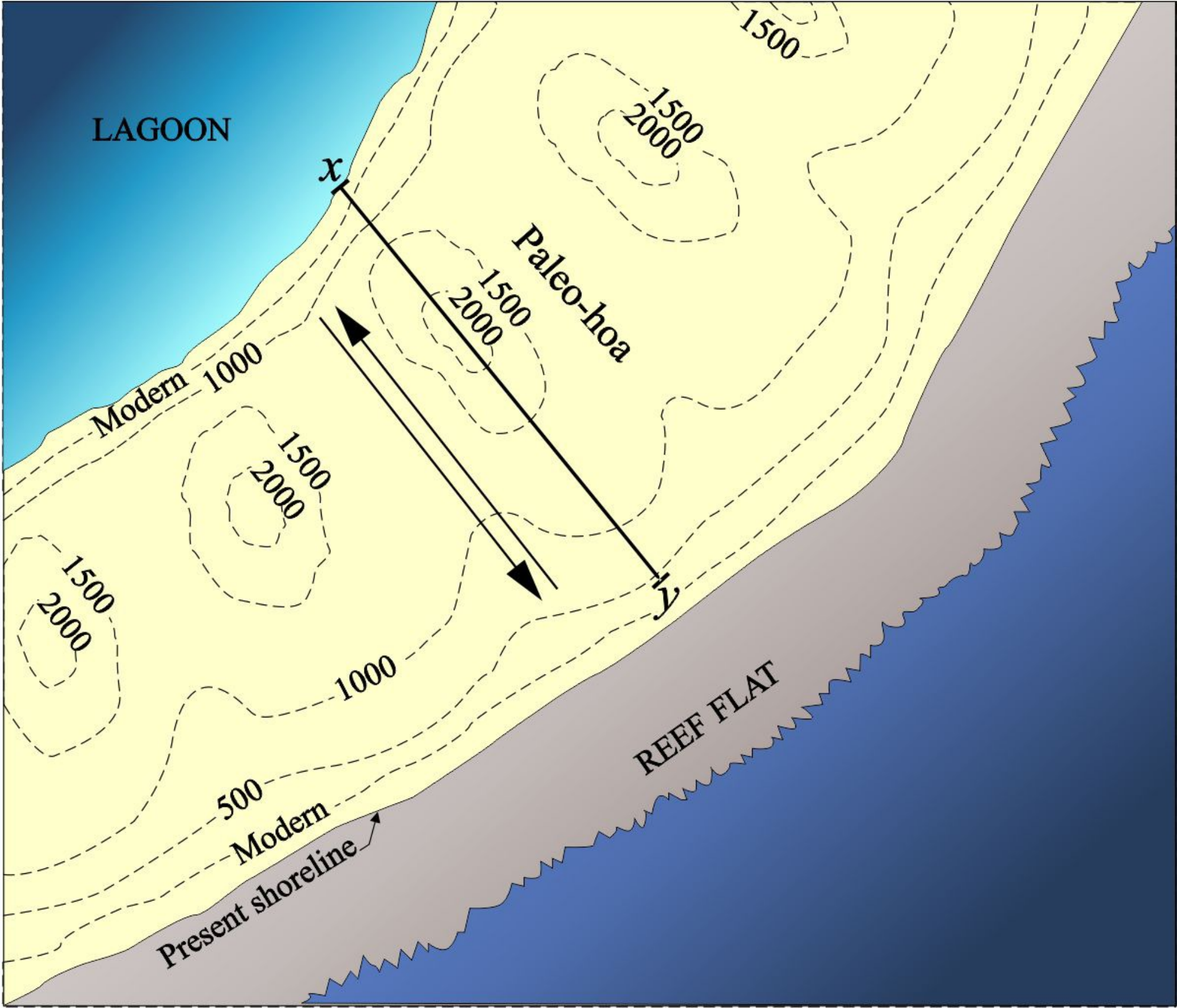
LAGOON
x
y
Paleo-hoa
1500
1500
2000
1500
2000
Modern
1000
1500
2000
1500
2000
1000
500
Modern
Present shoreline
REEF FLAT

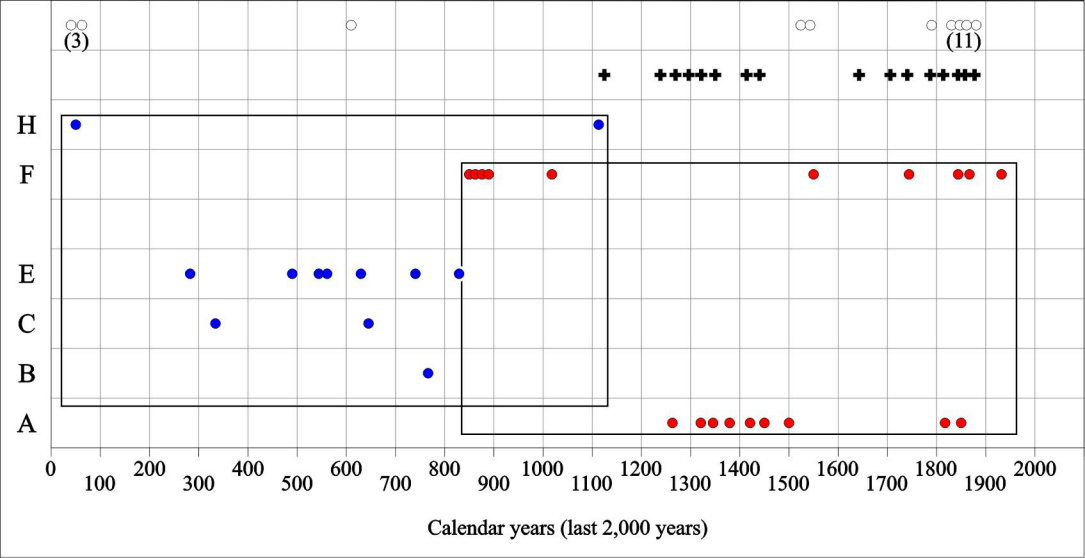
(3)
(11)
H
F
E
C
B
A
0
100
200
300
400
500
600
700
800
900
1000
1100
1200
1300
1400
1500
1600
1700
1800
1900
2000
Calendar years (last 2,000 years)

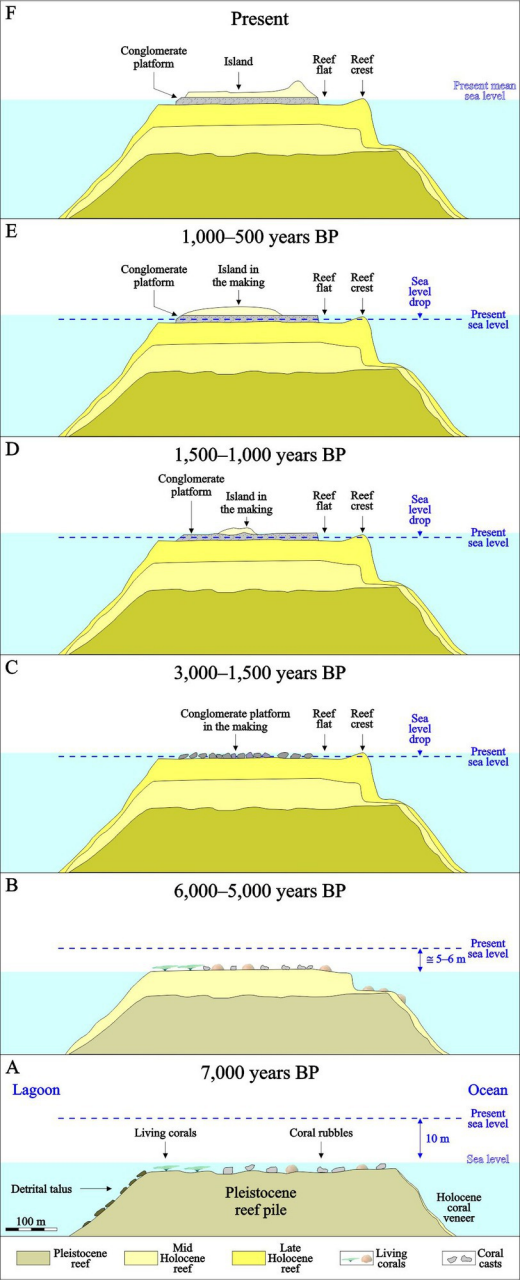
F
Present
Conglomerate platform
Island
Reef flat
Reef crest
Present mean sea level
E
1,000–500 years BP
Conglomerate platform
Island in the making
Reef flat
Reef crest
Sea level drop
Present sea level
D
1,500–1,000 years BP
Conglomerate platform
Island in the making
Reef flat
Reef crest
Sea level drop
Present sea level
C
3,000–1,500 years BP
Conglomerate platform in the making
Reef flat
Reef crest
Sea level drop
Present sea level
B
6,000–5,000 years BP
Present sea level
≅ 5–6 m
A
7,000 years BP
Lagoon
Ocean
Present sea level
Living corals
Coral rubbles
10 m
Sea level
Detrital talus
Pleistocene reef pile
Holocene coral veneer
100 m
Pleistocene reef
Mid Holocene reef
Late Holocene reef
Living corals
Coral casts

Codes	Samples	[^{238}U] ppm	[^{232}Th] ppb	$\delta^{234}U_m$(‰)	(^{230}Th/^{238}U)	(^{230}Th/^{232}Th)	$\delta^{234}U_i$ (‰)	Ages Cor yr BP
Excavation A								
7813	**Exc. A – SAT 64 A**	2.240 ± 0.018	0.133 ± 0.001	145.3 ± 1.8	0.00641 ± 0.00008	310.4 ± 4.2	145.5 ± 1.8	**600 ± 16**
7814	**Exc. A – SAT 64 B**	2.621 ± 0.021	0.149 ± 0.001	147.1 ± 1.7	0.00601 ± 0.00007	324.2 ± 3.8	147.3 ± 1.7	**562 ± 14**
7815	**Exc. A – SAT 66 A**	2.492 ± 0.020	0.115 ± 0.001	147.9 ± 1.3	0.00548 ± 0.00006	364.0 ± 4.3	148.1 ± 1.3	**513 ± 12**
7816	**Exc. A – SAT 68 A**	2.237 ± 0.018	0.124 ± 0.001	146.1 ± 1.3	0.00175 ± 0.00005	97.1 ± 3.0	146.2 ± 1.3	**156 ± 12**
7860	**Exc. A – SAT 68 B**	2.793 ± 0.022	0.149 ± 0.001	146.2 ± 1.3	0.00214 ± 0.00005	123.0 ± 2.6	146.3 ± 1.3	**193 ± 10**
7861	**Exc. A – SAT 71 A**	2.660 ± 0.021	0.194 ± 0.002	145.2 ± 1.5	0.00800 ± 0.00007	335.1 ± 3.1	145.5 ± 1.5	**750 ± 16**
7862	**Exc. A – SAT 71 B**	2.564 ± 0.021	0.118 ± 0.001	146.2 ± 1.2	0.00742 ± 0.00007	491.5 ± 4.6	146.5 ± 1.2	**700 ± 13**
7863	**Exc. A – SAT 73 A**	3.268 ± 0.026	0.093 ± 0.001	145.6 ± 1.4	0.00671 ± 0.00003	724.5 ± 3.7	145.9 ± 1.4	**636 ± 7**
7864	**Exc. A – SAT 73 B**	2.395 ± 0.019	0.114 ± 0.001	148.2 ± 1.4	0.00718 ± 0.00007	461.3 ± 4.3	148.5 ± 1.4	**676 ± 13**
7865	**Exc. A – SAT 74**	2.492 ± 0.020	0.162 ± 0.001	145.2 ± 1.2	0.06767 ± 0.00024	3180.8 ± 11.2	147.9 ± 1.2	**6629 ± 38**
Excavation B								
7725	**Exc. B – SAT 52 A**	2.703 ± 0.022	0.0398 ± 0.0003	145.0 ± 0.7	0.01298 ± 0.00011	2690.8 ± 22.2	145.5 ± 0.7	**1243 ± 12**
7726	**Exc. B – SAT 52 B**	3.095 ± 0.025	0.051 ± 0.001	139.4 ± 1.8	0.01327 ± 0.00009	2474.6 ± 17.7	139.9 ± 1.8	**1276 ± 13**
7727	**Exc. B – SAT 53 A**	2.545 ± 0.021	0.0326 ± 0.0003	135.5 ± 1.9	0.01292 ± 0.00010	3086.6 ± 23.4	136.0 ± 1.9	**1247 ± 13**
7728	**Exc. B – SAT 53 B**	2.593 ± 0.021	0.0355 ± 0.0003	143.0 ± 1.5	0.01577 ± 0.00011	3526.5 ± 25.2	143.6 ± 1.6	**1515 ± 15**
7729	**Exc. B – SAT 55 A**	2.257 ± 0.018	0.0414 ± 0.0004	142.8 ± 1.5	0.01307 ± 0.00014	2189.0 ± 22.9	143.3 ± 1.5	**1253 ± 17**
7730	**Exc. B – SAT 55 Bi**	2.283 ± 0.022	0.0425 ± 0.0004	141.2 ± 3.9	0.01480 ± 0.00013	2435.4 ± 22.0	141.8 ± 4.0	**1422 ± 20**
7731	**Exc. B – SAT 55 Be**	4.032 ± 0.033	0.0474 ± 0.0004	140.7 ± 2.2	0.01499 ± 0.00009	3900.2 ± 24.0	141.2 ± 2.2	**1442 ± 13**
7732	**Exc. B – SAT 57 A**	2.575 ± 0.021	0.0350 ± 0.0003	141.6 ± 1.5	0.01306 ± 0.00011	2954.8 ± 24.1	142.1 ± 1.5	**1254 ± 14**
7733	**Exc. B – SAT 57 B**	2.486 ± 0.020	0.827 ± 0.007	144.2 ± 1.7	0.01799 ± 0.00022	166.4 ± 2.0	144.9 ± 1.8	**1658 ± 60**
7734	**Exc. B – SAT 60 A**	2.583 ± 0.021	0.113 ± 0.001	137.1 ± 1.9	0.02687 ± 0.00015	1873.7 ± 10.8	138.1 ± 1.9	**2601 ± 25**
7735	**Exc. B – SAT 61 A**	2.752 ± 0.022	0.0448 ± 0.0004	145.6 ± 1.8	0.03113 ± 0.00016	5873.7 ± 30.4	146.8 ± 1.8	**3004 ± 23**
7736	**Exc. B – SAT 119 A**	2.255 ± 0.018	1.285 ± 0.010	137.4 ± 1.9	0.04962 ± 0.00025	265.6 ± 1.4	139.2 ± 1.9	**4743 ± 95**
Excavation C								
7802	**Exc. E – SAT 30 A**	2.574 ± 0.021	0.093 ± 0.001	146.5 ± 0.8	0.01447 ± 0.00009	1228.6 ± 7.2	147.1 ± 0.8	**1379 ± 13**
7803	**Exc. C – SAT 33 A**	2.872 ± 0.023	0.0524 ± 0.0004	145.7 ± 0.7	0.01433 ± 0.00010	2406.9 ± 11.6	146.2 ± 0.7	**1370 ± 12**
7804	**Exc. C – SAT 33 B**	2.655 ± 0.021	0.0507 ± 0.0004	142.9 ± 1.9	0.01752 ± 0.00011	2826.3 ± 12.8	143.6 ± 1.9	**1683 ± 16**
7805	**Exc. C – SAT 34 A**	2.817 ± 0.023	0.0555 ± 0.0004	145.4 ± 1.6	0.02506 ± 0.00009	3887.9 ± 8.3	146.4 ± 1.6	**2411 ± 15**
7806	**Exc. C – SAT 34 B**	3.100 ± 0.025	0.0278 ± 0.0002	145.0 ± 1.5	0.02733 ± 0.00008	9347.1 ± 18.8	146.1 ± 1.5	**2635 ± 12**
7773	**Exc. C – SAT 36 A**	2.766 ± 0.022	0.0094 ± 0.0001	145.9 ± 1.2	0.02447 ± 0.00006	21947.5 ± 52.3	146.9 ± 1.2	**2356 ± 8**
7774	**Exc. C – SAT 36 B**	2.570 ± 0.021	0.0159 ± 0.0001	143.6 ± 1.2	0.02423 ± 0.00008	11909.7 ± 39.5	144.5 ± 1.2	**2337 ± 11**
7807	**Exc. C – SAT 37 A**	2.475 ± 0.020	0.079 ± 0.001	144.1 ± 0.8	0.05147 ± 0.00013	4951.8 ± 12.0	146.1 ± 0.8	**5016 ± 19**
Excavation E								
7797	**Exc. E – SAT 42 A**	2.830 ± 0.023	0.042 ± 0.0003	146.2 ± 1.0	0.01527 ± 0.00006	3116.5 ± 12.1	146.8 ± 1.0	**1461 ± 9**
7798	**Exc. E – SAT 44 A**	0.532 ± 0.004	0.074 ± 0.001	144.7 ± 0.9	0.01832 ± 0.00033	406.3 ± 7.2	145.4 ± 0.9	**1732 ± 48**
7799	**Exc. E – SAT 47 A**	2.606 ± 0.021	0.045 ± 0.0004	144.7 ± 1.1	0.01233 ± 0.00006	2180.8 ± 8.4	145.2 ± 1.1	**1180 ± 10**
7800	**Exc. E – SAT 47 B**	2.726 ± 0.022	0.052 ± 0.0004	144.9 ± 1.9	0.01329 ± 0.00005	2157.0 ± 6.6	145.4 ± 1.9	**1271 ± 9**
7775	**Exc. E – SAT 48 A**	2.681 ± 0.021	0.019 ± 0.0002	143.7 ± 1.6	0.01587 ± 0.00005	6844.1 ± 23.7	144.3 ± 1.6	**1525 ± 8**
7776	**Exc. E – SAT 48 B**	2.520 ± 0.020	0.018 ± 0.0001	145.1 ± 1.0	0.01531 ± 0.00008	6635.4 ± 33.2	145.7 ± 1.0	**1469 ± 9**
7801	**Exc. E – SAT 50 A**	2.788 ± 0.022	0.044 ± 0.0004	145.1 ± 0.9	0.02707 ± 0.00007	5266.9 ± 13.2	146.2 ± 0.9	**2608 ± 11**
Excavation F								
7759	**Exc. F – SAT 77 A**	2.178 ± 0.017	0.087 ± 0.001	145.9 ± 0.9	0.00083 ± 0.00005	63.0 ± 3.9	146.0 ± 0.9	**71 ± 10**
7760	**Exc. F – SAT 77 B**	2.918 ± 0.023	0.011 ± 0.0001	146.6 ± 1.5	0.00171 ± 0.00004	1334.5 ± 30.7	146.7 ± 1.5	**163 ± 5**
7761	**Exc. F – SAT 79 A**	2.690 ± 0.022	0.048 ± 0.0004	145.2 ± 1.6	0.00146 ± 0.00005	249.9 ± 9.3	145.2 ± 1.6	**136 ± 7**
7762	**Exc. F – SAT 79 B**	2.326 ± 0.019	0.293 ± 0.002	145.0 ± 1.5	0.00306 ± 0.00009	74.1 ± 2.2	145.1 ± 1.5	**266 ± 23**
7763	**Exc. F – SAT 81 B**	2.698 ± 0.022	0.041 ± 0.0003	145.2 ± 1.5	0.00977 ± 0.00010	1969.0 ± 19.3	145.6 ± 1.5	**933 ± 12**
7764	**Exc. F – SAT 81 A**	2.765 ± 0.022	0.042 ± 0.0003	144.1 ± 0.9	0.00477 ± 0.00004	945.3 ± 7.3	144.3 ± 0.9	**453 ± 6**
7765	**Exc. F – SAT 82 A**	2.440 ± 0.020	0.173 ± 0.001	144.5 ± 0.7	0.01224 ± 0.00007	526.6 ± 3.0	145.0 ± 0.7	**1159 ± 15**
7766	**Exc. F – SAT 82 B**	2.438 ± 0.020	0.177 ± 0.001	142.6 ± 3.0	0.01208 ± 0.00008	505.6 ± 3.2	143.0 ± 3.0	**1146 ± 19**
7767	**Exc. F – SAT 83 A**	2.627 ± 0.021	0.144 ± 0.001	144.0 ± 2.6	0.01226 ± 0.00006	673.9 ± 3.5	144.5 ± 2.6	**1165 ± 15**
7768	**Exc. F – SAT 83 B**	3.272 ± 0.026	0.220 ± 0.002	143.0 ± 1.7	0.01231 ± 0.00006	546.4 ± 2.6	143.4 ± 1.7	**1167 ± 15**
7769	**Exc. F – SAT 86 A**	2.497 ± 0.020	0.281 ± 0.002	143.4 ± 1.9	0.01207 ± 0.00007	323.3 ± 2.0	143.9 ± 1.9	**1135 ± 22**
7770	**Exc. F – SAT 86 B**	2.479 ± 0.020	0.018 ± 0.0001	147.4 ± 0.9	0.01183 ± 0.00007	4973.6 ± 28.9	147.8 ± 0.9	**1131 ± 8**
7771	**Exc. F – SAT 87 A**	3.991 ± 0.032	0.021 ± 0.0002	144.0 ± 1.0	0.02431 ± 0.00006	13765.3 ± 32.8	145.0 ± 1.0	**2344 ± 8**
Excavation G								
7793	**Exc. G – SAT 91 A**	2.858 ± 0.023	0.114 ± 0.001	145.3 ± 1.3	0.02463 ± 0.00007	1891.1 ± 3.8	146.3 ± 1.3	**2366 ± 15**
7794	**Exc. G – SAT 91 B**	4.149 ± 0.034	0.170 ± 0.001	146.5 ± 1.6	0.03074 ± 0.00008	2301.1 ± 5.0	147.8 ± 1.6	**2958 ± 17**
7795	**Exc. G – SAT 93 A**	2.733 ± 0.022	0.034 ± 0.0003	145.5 ± 0.8	0.02488 ± 0.00006	6043.1 ± 15.4	146.5 ± 0.8	**2395 ± 10**
7796	**Exc. G – SAT 93 B**	2.692 ± 0.022	0.029 ± 0.0002	145.3 ± 1.0	0.02449 ± 0.00005	7059.2 ± 15.0	146.2 ± 1.0	**2358 ± 8**
7748	**Exc. H – SAT 94 a**	2.177 ± 0.017	0.105 ± 0.001	142.8 ± 1.3	0.04811 ± 0.00010	3064.5 ± 6.5	144.7 ± 1.3	**4683 ± 21**
Excavation H								
7747	**Exc. H – SAT 96 A**	2.091 ± 0.017	0.735 ± 0.006	143.8 ± 0.9	0.02699 ± 0.00013	235.8 ± 1.2	144.9 ± 0.9	**2531 ± 53**
7746	**Exc. H – SAT 97 A**	3.059 ± 0.025	0.115 ± 0.001	145.2 ± 0.9	0.00845 ± 0.00008	690.6 ± 6.9	145.5 ± 0.9	**801 ± 13**
7808	**Exc. H – SAT 99 B**	3.342 ± 0.027	0.046 ± 0.0004	144.2 ± 1.0	0.02043 ± 0.00006	4488.5 ± 13.6	145.0 ± 1.0	**1965 ± 9**
7809	**Exc. H – SAT 99 A**	2.330 ± 0.019	0.041 ± 0.0003	146.4 ± 0.7	0.02229 ± 0.00007	3905.9 ± 12.8	147.2 ± 0.7	**2140 ± 10**
7810	**Exc. H – SAT 100A**	2.978 ± 0.024	0.125 ± 0.001	144.5 ± 1.1	0.02952 ± 0.00009	2158.3 ± 6.3	145.7 ± 1.1	**2843 ± 16**
7811	**Exc. H – SAT 101A**	5.029 ± 0.041	0.068 ± 0.001	143.5 ± 0.7	0.02342 ± 0.00006	5339.0 ± 13.2	144.4 ± 0.7	**2257 ± 8**

Windward sites				Leeward sites			
Excavation A				**Excavation F**			
SAT 64A	1419	±	16	SAT 77A	1948	±	9.5
SAT 64B	1457	±	14	SAT 77B	1856	±	4.5
SAT 66A	1506	±	12	SAT 79A	1882	±	7
SAT 68A	1864	±	11.5	SAT 79B	1753	±	22.5
SAT 68B	1826	±	10	SAT 81A	1566	±	5.5
SAT 71A	1269	±	16	SAT 81B	1085	±	12
SAT 71B	1320	±	12.5	SAT 82A	859	±	15
SAT 73A	1383	±	7	SAT 82B	873	±	18.5
SAT 73B	1344	±	12.5	SAT 83A	854	±	14.5
Excavation B				SAT 83B	851	±	15
SAT 52A	776	±	12.5	SAT 86A	884	±	21.5
Excavation C				SAT 86B	888	±	8.5
SAT 33A	648	±	12	**Excavation H**			
SAT 33B	336	±	15.5	SAT 97A	1217	±	13
Excavation E				SAT 99B	53	±	9.5
SAT 30A	639	±	13				
SAT 42A	557	±	9				
SAT 44A	286	±	48				
SAT 47A	839	±	9.5				
SAT 47B	747	±	9				
SAT 48A	493	±	8				
SAT 48B	550	±	9.5				